
Design of an experimental set-up for research into the hydrodynamics of insect-like water surface locomotion

---

James Maybey

18/05/2023

Dr. Swathi Krishna, Desmond Lim

Word Count: 10,499

Pages: 70

This report is submitted in partial fulfilment of the requirements for the Mechanical Engineering with Automotive Engineering, Faculty of Engineering and Physical Sciences, University of Southampton

Decleration:

I, James Maybey declare that this thesis and the work presented in it are my own and has been generated by me as the result of my own original research.

I confirm that:

1. This work was done wholly or mainly while in candidature for a degree at this University;

2. Where any part of this thesis has previously been submitted for any other qualification at this University or any other institution, this has been clearly stated;

3. Where I have consulted the published work of others, this is always clearly attributed;

4. Where I have quoted from the work of others, the source is always given. With the exception of such quotations, this thesis is entirely my own work;

5. I have acknowledged all main sources of help;

6. Where the thesis is based on work done by myself jointly with others, I have made clear exactly what was done by others and what I have contributed myself;

7. None of this work has been published before submission.

Acknowledgements:

I thank my supervisor Dr. Swathi Krishna for supporting my work and giving me guidance during my project. I also am grateful for being given the opportunity to work on this project by Dr. Krishna. I further thank Desmond Lim for offering his additional time and support on this project. I lastly thank my Father for helping me and giving me the motivation to continue with my work.

Abstract:

Many studies have been made over time into the motion employed by insects' wings. The latest motions to be studied need to be replicated and analysed by employing an experimental apparatus. A vast number of set-ups exist with the sole purpose of recreating the flapping motion of wings, and from these, results can be found and implemented into robotic application. Unmanned vehicles in both air and water would benefit greatly from the planned future research. The hydrofoiling of honeybee's wings will allow for a great new deal of design possibilities, with existing ideas for implementation in drone recovery.

This paper outlines the design of an experimental piece of equipment that will allow the modelling of a wing in a water environment. The equipment will be designed to have both a pitch and stroke motion, both with independent control systems. The design will be used for future experimentation in both static and flowing water and this is when the testing and results data will be collected. The pitching mechanism is controlled with a pair of bevel gears and outputted from a stepper motor. A second stepper motor will drive the stroke motion however will use a timing belt pulley system to deliver this output.

The future testing will involve the use of a force-torque sensor that will allow the studying of related forces experienced throughout the stages of the honeybee's motion. These forces can be used to produce useful coefficients and allow for future optimization to idealise said coefficients.

The design was inspired from existing apparatus outlined in Section 2 of the report (Background). These existing designs allowed for a stable foundation to develop upon in an iterative manner.

Nomenclature:

Angle of attack, α (°)

Area, A (m^2)

Chord length (wing), c (m)

Coefficient of Drag, C_D

Coefficient of Lift, C_L

Coefficient of Power. C_P

Density, ρ (kg/m^3)

Distance to axis of rotation, R_0 (m)

Force, F (N)

Frequency, f (Hz)

Span length (wing), R (m)

Torque, T (Nm)

Velocity of free stream flowing fluid (Lab+motion), U_{inf} (m/s)

Speed of free stream flowing fluid (Lab apparatus speed), V_{inf} (m/s)

List of Figures:

List of Tables:

List of Abbreviations:

AR: Aspect Ratio

CAD: Computer-Aided Design

Eq: Equation

FEA: Finite Element Analysis

HTD: High-Torque Drive

HUAV: Hybrid Underwater-Aerial Vehicles

ID: Inner Diameter

MAV: Micro Air Vehicle

OD: Outer Diameter

PIV: Particle Image Velocimetry

RWT: Recirculating Water Tunnel

UAV: Unmanned Aerial Vehicle

UAAV: Unmanned Aerial-Aquatic Vehicle

UV: Underwater Vehicle

Contents:

1. Introduction:

1.1. Big picture:

Honeybee's have recently been found to use their wings to perform a version of surface locomotion that involves moving their wings back and forward across the water-air boundary to create a hydrofoiling effect. This effect means that when the honeybee's land on their underside on the water surface they can propel themselves forward and move towards dry land. Investigating this motion may allow for experimental research to be made into replicating this motion and then implementing it into mechatronics. With Unmanned Aerial-Aquatic Vehicles (UAAVs) predominantly using jet-thrust or rotor propulsion to create their forward motion, this method would exist as a backup system separate to the primary motion. Jet and rotor propulsion allow reliable and rapid manoeuvring, capable of leaving and landing on the water surface whereas the honeybee's motion will only be applicable to the water surface locomotion. This therefore narrows the motion's applicability down to solely aquatic movement, most likely presenting as a backup recovery motion usable when a UAAV malfunctions and crashes to the water's surface.

This project will focus on the design of an experimental apparatus that can model the sinusoidal motion of the wing and produce measurable values of forces and torques created by the movement. The forces and torques surrounding the motion will determine its viability in implementation in the future. The apparatus will also leave the possibility for future variation and customisation to allow experiments with a variety of wing shapes and aspect ratios. The design process will include the use of Computer-Aided Design (CAD) to show the stages of design development and illustrate the decisions made along the way, this will include the component choices and assembly methods.

1.2. Aims and Objectives:

The overall aim of this project is to design and create an apparatus capable of yielding model results that are relevant and transferable. This comes with project design constraints like target capabilities (e.g., fine resolution) and also additional limitations like budgeting. The project will also be broken down into smaller objectives, these include the deciding of mechanisms that will deliver the motion, the choice of electronic and motion transmission components and lastly finalising a design that is fully capable of assembly to process onto manufacture.

1.3. Report Structure:

This report will be structured by initially performing research into the existing literature surrounding the topic. This will allow the ability to outline the expected motion, the

methods of modelling, existing apparatus and UAAVs and the potential utility. Following the literature review, the next area for design constraints come from the location and environments the apparatus will be testing in. This includes planning through the future experimentation and methodology to allow for the design to be suitable for fixing to the lab equipment like static water tanks and water flumes. Using these two rounds of research it is possible to create a brief specification for what the apparatus aims to achieve and will be constrained by. From these constraints, beginning with initial sketching, the developmental design process will start. In this process, design decisions will be made on the methods of power transmission and how the motion will be delivered. The final design is summarised and key aspects outlined. This includes the justification of design decisions along the way, including the components by using investigative torque calculations to ensure the motors will be capable of delivering the required output. The electronics that control the system are then outlined and briefly explained. The final stage includes the manufacturing review, explaining the differences between the planned design and manufactured rig. The report ends with a conclusion and discussion on the future work from this project.

2. Background:

The purpose of the background chapter is to investigate the existing information available that has brought on or influences the project's experimental design. Background will cover the paper and context that has brought on the need for the apparatus, existing experimental rigs and modelling used in flapping wing experimentation, existing mechatronic applications the research could be used for, and lastly outlining the future experimentation planned for the rig. The chapter will end with a summary of what was learned from the chapter.

2.1 Project Inspiration

2.1.1. Key literature:

The research's key inspiration is 'honeybees use their wings for water surface locomotion' by Chris Roh et al. which is centred around analysing the honeybee's motion. [1] This includes proving that the method observed is using hydrofoiling as the source of thrust and is therefore different to other forms of bio-locomotion methods found in insects (like rowing). The report manages this by analysing a honeybee on the water's surface and using Particle Image Velocimetry (PIV) to measure the momentum imparted by the wings to the water. Figure 2.1 shows an example PIV setup using a laser and camera to study the affect of flow over a wing section. PIV studies how the particles in the fluid are moving which can then be analysed to obtain useful data.

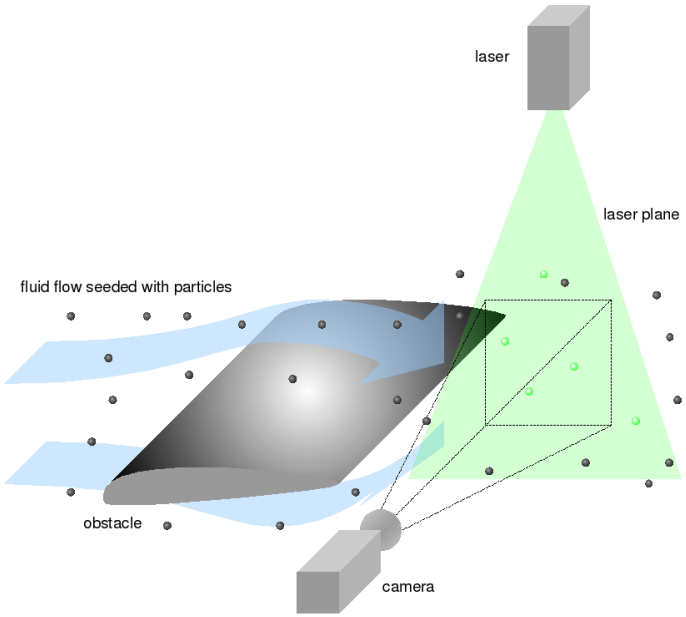

Figure 2.1: Example PIV experimentation [2]

The results of testing showed that the momentum created was comparable in magnitude to the ~20μN required to overcome hydrodynamic drag [1]. This data is found by studying the live bee's motion; however, we will aim to use a robotic mechanism to

model the motion of the wing and scale the results after. Working with a mechanism instead of live bees avoids ethics problems and creates controllable repeatable results. Investigating other locomotion methods like rowing shows distinct differences that are outlined by the paper and with winged UAAV designs already out there, the hydrofoiling motion is a far newer and more appealing motion to implement. With wings already featured in many designs, allowing both flight and water locomotion, rowing is made redundant as the need for fixed legs on the surface is made obsolete.

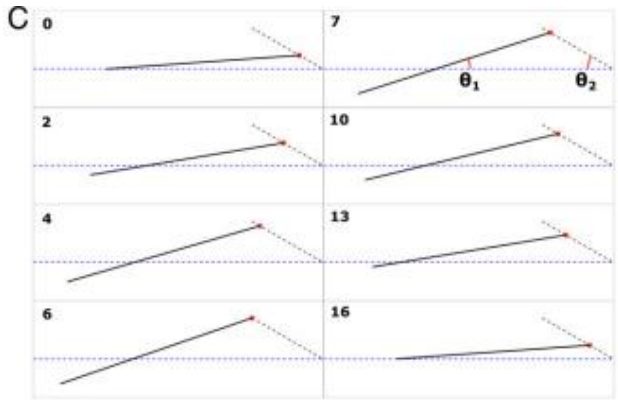

Figure 2.2: Pronate and supinate motion of honeybee wings [1]

Figure 2.2 displays the pronating and supinating that defines the honeybee's hydrofoiling motion. The stroke amplitude whilst the bee rests on the water surface is different to that displayed in air, in air it is shown to have a stroke amplitude of approximately 90° [3] whereas the study shows less than 10° on water. It also labels the angles of attack which can then be measured and graphed through the progression of the motion as shown in figure 2.3.

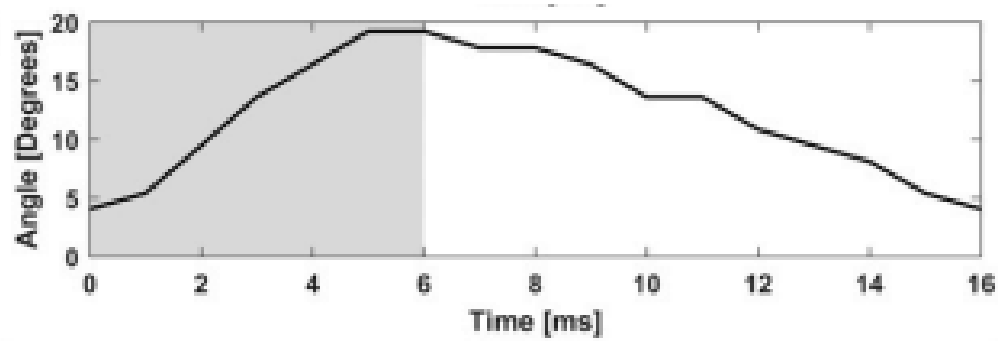

Figure 2.3: Angle of attack, α, vs. time [1]

This helps us define a range of angle of attack, α that the experimental rig should be capable of. Although the motion falls below 20 degrees at its peak, it is worth being capable of a wider range to allow for further analyses and optimisation to find the angles of attack that maximise power and lift coefficients. It is also stated in the report that if the

wing could detach from the water surface during the power stroke, the recovery stroke could avoid implementing adverse thrust. [1] This means that the rig could not only replicate the biological motion of the bee, but test for more efficient forms.

2.1.2. Water surface locomotion:

The paper also compares other water surface locomotion techniques like rowing. Rowing uses hydrophobic legs to sweep or step and propel the insect or drone forward along the water. The distinction is made that the power strokes of water walking and honeybees differ as they occur striking down on the water and lifting the water surface respectively. [1] There is also mention of insects using alternate biolocomotion like chemically driven propulsion. [1] The method of rowing (or galloping) and walking are methods that can be found in a variety of spiders that also recalls the utilisation of hydrophobic limbs to not break the water's surface tension and stay fixed upon the air-water boundary. [4]

The paper finally mentions the future application the study has for robotics. The potential for an aerial-aquatic hybrid vehicle to use this motion as a its thrust source in both air and on the surface of a body of water can be explored with future research and design development following further modelling to maximise thrust outputs.

2.2. Previous Apparatus and Modelling Methods:

2.2.1 Existing Experimental Rigs

In the paper, to recreate the wing kinematics, a flexible wing with span of 6.4mm chord and 19.2mm span was made with an aspect ratio (AR) of 3, and by combining this with a function generator to power and control the wing, the motion could be replicated.

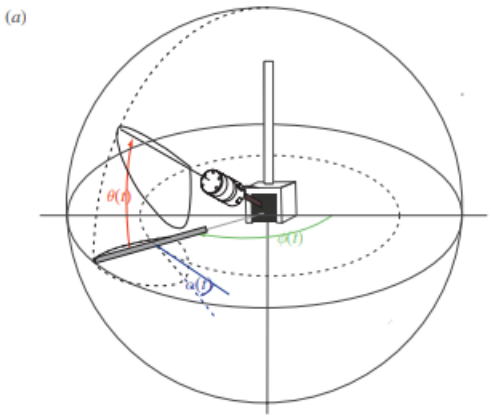

Figure 2.4: Flapping wing experimental set-up [5]

Zhao et al. features the use of an existing experimental set-up (shown in figure 2.4) to model the flapping of wings. The design featured a bevel gear wrist that was used to actuate the wing angle and displayed the limitation of ±45° for the stroke angle due to the

geometry of the gearbox. [6] This design however utilises more degrees of freedom then we are aiming to test for. The apparatus we aim to design will only model the stroke and pitching of the bee's wing whereas this model has an additional flapping motion that complicates the design and introduces this limitation. The design varied α from -9 to 90° in 4.5° increments, this corresponds to a total of 23 different controllable positions through the motion. [7] The experimental rig that we aim to design should aim to model its range of motion in a greater number of steps to allow for closer analysis of α and the forces involved in each wing position. This papers main focus was on the flexibility of the wing and the effect on flapping wings. With the possibility of future flexible wing research, it would be beneficial for the apparatus we design to be capable of changing out its testing wing. Using separate adapter designs to fix the type of wing to the chosen force and torque sensor is the easiest way to provide this.

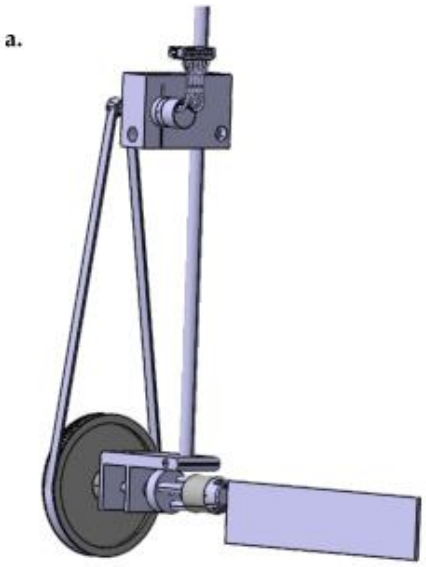

Figure 2.5: Flapping wing apparatus used to model stroke and pitch motion [6]

Figure 2.5 illustrates another existing apparatus that uses a pulley belt transmission system to control the pitch and a rotating main shaft to deliver a stroke motion. This combination is the most basic solution to delivering these two positional outputs and should be heavily considered for implementation into our apparatus. Although this rig was submerged for its use, the implementation of pulleys going through the water surface could not only disturb the water but also possibly lead to slipping or lack of effective power transmission. The design uses an ATI Nano17 force-torque sensor to measure and record their results from their experimentation and this is a design component that should also be considered for use. [6]

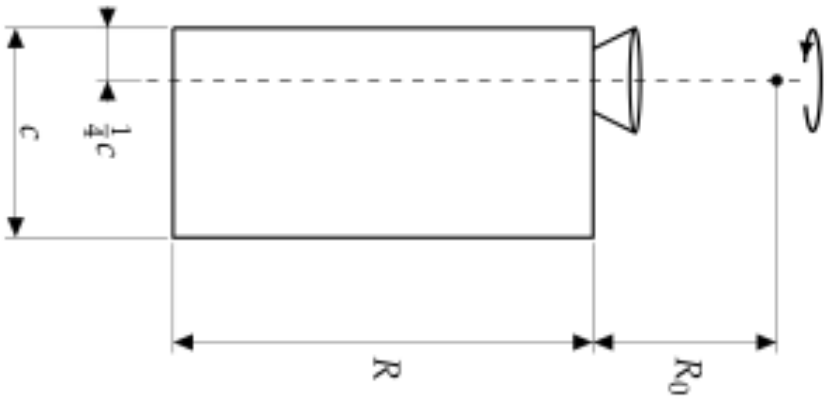

Figure 2.6: Dimensions of rectangular plate used to model the wing in hover [6]

Figure 2.6 outlines how the axis of pitching lies a quarter of the chord length, c, away from the leading edge, and further outlines R_0 as the distance from the base of the wing to the axis of the stroke motion. R_0 will vary with the apparatus' design, however, the distance c/4 is independent to the rig design and could be used in our modelling. Appendix A shows some of the changes experienced in robotic flapping hovering flight with the pitch axis at a quarter chord position and a half chord position, from these results it is likely we will also decide to use this c/4 distance. [7]

Table 1. Wing parameters of three flying insects and the scaled model submerged in water with $\nu_{20^\circ C} = 1.00 \times 10^{-6}\,m^2\,s^{-1}$.

Parameters			Honeybee [3]	Hawkmoth [3]	Hoverfly [32]	Model [31]
Wing stroke frequency	f	(Hz)	232	26	166	0.25
Wing chord	c	(mm)	3	18.3	2.4	34
Wing span	R	(mm)	10	48.3	9.03	107
Stroke amplitude	2ϕ	(°)	91	115	148.2	180
Reduced frequency	k		0.3	0.3	0.32	0.32
Reynolds number	Re		1412	5885	620	2510

Table 2.1: Wing parameters of three flying insects and the scaled model submerged in water with $v_{20^\circ C} = 1.00 \times 10{-}6\ m^2\ s^{-1}$ [6]

Table 2.1 provides us with a wing chord, c and span, R, that could be used in our first round of experimentation. Although, our apparatus will allow for the substitution of wing design, starting with a wing chord of 34mm and span of 107mm allows for the results of this study to be replicated and compared if required, however variations may arise from differences in the rig design and how this interacts with the fluid environment.

Finally, from this paper we can recall the equations for the coefficients of lift, drag and power that will be calculated using our results. These are listed in Eq(1) below.

$$C_L = \frac{L}{\frac{1}{2}\rho R c \overline{U}^2}, \quad C_D = \frac{D}{\frac{1}{2}\rho R c \overline{U}^2}, \quad C_P = \frac{P}{\frac{1}{2}\rho R c \overline{U}^3}.$$

Equation 1: Equations to calculate coefficient of lift, drag and power.

Using these equations, it is possible to study the motion's efficiency, which quantifies the lift-to-effort ratio. Using a compilation of computer software, the apparatus' collected results can be optimized in the future to maximize these coefficients and improve the motion's effectiveness. Another study by the same authors utilises a different mechanism design to model flapping wings, this time using a bevel gear pair to control the pitching motion and a pulley system to drive the stroke.

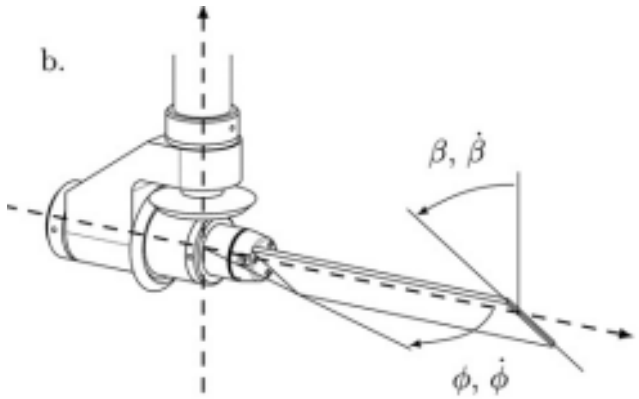

Figure 2.7: Experimental set-up using to bevel gears [8]

Figure 2.7 shows the use of an outer shaft coupled to a 'mechanism block' that holds the wing's axle that provides the pitching motion. The bevel gears suggest that the design uses an inner and outer shaft that will be driven independently, one controlling the stroke and one the pitch. The inner shaft passes the full length of the tube and fixes to a bevel gear that is used in a pair to then rotate the wing axle and control the wing's α. With components expected to be partially or fully submerged, the bevel gears design appears far more appealing compared to the pulley, as there would be no chances of slipping or reduction in torque. These designs are also, far more suitable than that shown in Zhao et al. as they do not have such limitation in stroke amplitude, allowing for a minimum 180° (compared to 90°), being restrained only by the sensor wire.

2.2.2. Wing Modelling:

To achieve results that can be considered comparable we need to prove that correct modelling methods are being chosen. Investigating the available methods of analysing wing responses show that using a straight leading edge on the wings 'are desirable for increased performance' [8], this alongside with the existing apparatus analysed in

Section 2.2.1 allows us to confidently chose a rectangular wing form. With existing plans to ensure the apparatus can substitute its chosen test wing, we will be able to confidently test a wide range of AR and also explore flexible wings. This gives the maximum opportunity for finding a wing shape that will produce the most thrust from the motion.

A variety of wing shapes and sizes could be used in our modelling but for the purpose of our initial testing, a specific wing must be chosen. It has already been seen from previous rigs that a rectangular wing, chord length of 34mm and span of 107mm is most likely to be used however this choice must be justified. Many studies into oscillating and flapping wings vary in their chosen AR. AR is defined as c/R and is a method of attributing the shape of the wing. One study based on flexible wings for Micro Air Vehicles (MAVs), used a range of 1 to 6 for their AR [10] whereas another study for underwater vehicles (UVs) used a range of 3 to 10. [11] Finally, a paper investigating the use of flexible flapping wings for Unmanned Aerial Vehicles (UAVs) used a wing of AR of 4 with 60mm chord length and 240mm span. [12] Although these three all serve for different applications; they reinforce the initially chosen AR of 3.15 and show strong support for this choice.

Future modelling and UAAV design may decide to use multiple oscillating hydrofoils, research into this has shown that there is little enhancement after a series of three, however this may change with modelling in different motions and with different hydrofoil spacings. [13]

2.3. UAAVs and MAVs

2.3.1. Existing UAAV designs and application potential:

UAAVs are a useful developing technology that has a strong variety of applications, including imaging, surveying, communication [14], checking oil spills [15], sample data collection like algae [16], and general water quality monitoring.[17] The bright advantage of the UAAVs is that they can find the samples, like an oil spill or a collection of algae from the air, land directly nearby and start sampling data, creating a more efficient method than currently used. They are most commonly powered by jet-thrust, propellers or flapping wings. [18]

The common issue with UAAVs is the struggle to leave the air-water boundary after landing, this is further complicated by vehicles that travel under the water's surface. To allow some designs to perform underwater, they require subsystems that drain and flood compartments when needed. [19]. In fixed wing designs this is because as the chord length increases for a set aerofoil section, the buoyancy force per unit span increases quadratically, making it challenging for the drone to stay submerged. [20] Another solution used is sets of propellers that output forces strong enough to not only drive the

drone through the water but also keep it submerged at the same time. [21] Hybrid Underwater-Aerial Vehicles (HUAVs) exist that incorporate both these features to overcome this issue. [22] There is wide variety of UAAV designs already being explored as shown below in table 2.2.

Robot name	Aircraft type	Water navigation	Key features
SUWAVE [16], [17]	Fixed-wing, rotorcraft	Water surface	VTOL
MEDUSA [14]	Quadcopter, jet-thruster	Underwater	Two agents, quadcopter, underwater pod
SailMAV [12]	Fixed-wing, sailing	Water surface	Morphing wing
AquaMAV [4], [7]	Fixed-wing, jet-thruster	Underwater	Morphing wing, plunge diving, wet launch
Aquatic jump-glider [15]	Fixed-wing, jet-thruster	Air glide, water surface	Multiple jumps, wet launch
ACAT [18], Flying Fish Solar-Powered [19]	Fixed-wing, seaplane	Water surface	Land on Water, running takeoff
Kollmorgen Sea Sentry 2009, Darpa Cormorant 2005 and XFC Sea Robin 2013 [20]	Fixed-wing, submarine launched	Underwater	dry launch, morphing wings
Beihang Flying Fish [21]	Fixed-wing, rotorcraft, jet-thruster	Underwater, surface	Morphing wings, wet launch, ballast
MIT flying fish [22]	Fish swimming (undulation)	Air glide, underwater	Underwater speed 5m/s
Quad-H2o, Mariner, HUAUV [23], Loon Copter [9]	Quadrotor	Underwater	Dual-propeller system
Flying jellyfish [24]	Ornithopters	Underwater, surface	Self stabilizing without sensors,
RoboBee [25]	Ornithopters	Underwater	Leaping out of water, micro scale

Table 2.2: Existing UAAV designs [23]

Table 2.2 shows the propulsion methods for the designs and with many of them using fixed-wings for aerial flight it leaves potential to mobilise the wings to implement the honeybee's motion and navigate the water surface with an alternate propulsion method.

2.3.2. MAVs potential:

Flapping wing research on insects is a consistently explored area and from this, robotic insect MAVs have been designed. [24] The advantage of MAV's is that they could be deployed in large numbers for search and sampling applications, however they hold no capability for payload or cargo. [25] MAVs are defined as being no greater than 15-20cm long [26] (for example the Delfly micro uses a 10cm wingspan [27]) and whilst we plan on modelling a greater wing, the results could be scaled to the smaller application. It is also reiterated the importance of not just copying the biological solutions for these drones but also then improving the motion to get the maximum efficiency from them. [27]

2.4. Future experimentation environment and methodology:

Future experimentation will occur at a University of Southampton (UOS) laboratory and first involve using the apparatus in a static water tank. The available tank is of measurements 1x1x2m and will be partially filled to a suitable length/depth depending on the apparatus design. The testing involves a lower torque requirement to run the apparatus through the water (in comparison to flowing water). A brief overview of the methodology involves first fixing the rig above the tank and then programming motors to create the desired motion and finally running the program whilst saving data from the force-torque sensor at a sampling frequency of 1000Hz [7]. The programmed motion can then be compared to the results over time to attribute results to α and stroke position. This applies to the second round of testing in a recirculating water tunnel (RWT) with the

difference being the addition of the water flowing at a set speed. The available RWT has an experimental test section measured 1.2x0.8x0.8m and allows a maximum flow speed of 1m/s. This 1m/s test limit allows us to design for the required torque to drive the apparatus in this environment and overcome the drag forces involved in the motion, however, in reality, the testing will initially be done at 0.3m/s and this is the speed we should design for. The forces will however depend on the wing area for the pitch motion and the apparatus area for the stroke motion.

The two experiments will allow for the finding of coefficients at individual points throughout the motion as mentioned in the previous literature. This will then allow for experimentation and optimization to get greater thrust and power from the motion. This then will allow for implementation into UAAV designs and future application. The Lab equipment used to test the apparatus will have no limitation for design height and requires only the correct frame to fix the apparatus to. This can be done using an arrangement of metal extrusion lengths fixed together that can be bolted to. The UOS lab equipment has an existing extrusion frame above the tanks and they will be the chosen point of mounting.

2.5. Background Summary:

The background research that has been covered will be what influences the final apparatus design criterion. From the research we learned a suitable modelling wing size to take forward and also the existing systems being used to create the motion. We can investigate the use of bevel gears and pulley systems as they are the most appealing and secure method of power transfer. Other gearing systems are available but are unlikely to be our first choice. The honeybee's motion, along with other insect's and bird's wing flapping, has been shown to be modellable using a harmonic sinusoidal function like a cosine wave. This could be coded into a software like MATLAB and inputted into a set of stepper motors. This also means that alongside two stepper motors, I will need two signal converters to process the cosine functions and allow the motors to output the motion. The range of the honeybee's wing positions can be broadly covered with a ±45° α and 90-180° stroke length and so this is the target capability for the design.

The research into existing UAAVs has shown how the data that will be collected from this apparatus will be used to developed new locomotion strategies and open up the possibility for a new wave of designs. MAVs are also a developing technology that could incorporate the movement on a smaller scale to benefit its design issues. UAAVs have a wide variety of uses in the future of automation and research, therefore the potential beneficial impact the future research could have is large.

Finally, by planning ahead the future methodology of experimentation, it was found the lab equipment and testing implemented only minor design constraints like the overall height of the apparatus to allow sufficient submersion into the tanks and the planned modelling speed of the flowing water in the RWT. With this, all the required information has been collated and is ready to be taken forward into the design process.

3. Developmental Design Process:

Taking inspiration from the previous experimental apparatus, initial design drawings could be made to investigate some variations of the key design features like the arrangement of the bevel gear assembly and the mounting of the sensor. These initial drawings are then developed into CAD models depicting the exact scaled components used in the final rig. Analysis into the implementation and effectiveness of key design features are made and then a final component material is chosen. Brief validation is made, comparing the final design to any targets made in the Section 2.

3.1. Initial sketches:

Using figure 2.7 as the initial inspiration, sketches were made to investigate possible design solutions to the complicated assembly required to achieve such a design. This included the ability to provide torque down to the bevel gears without the issue of backlash.

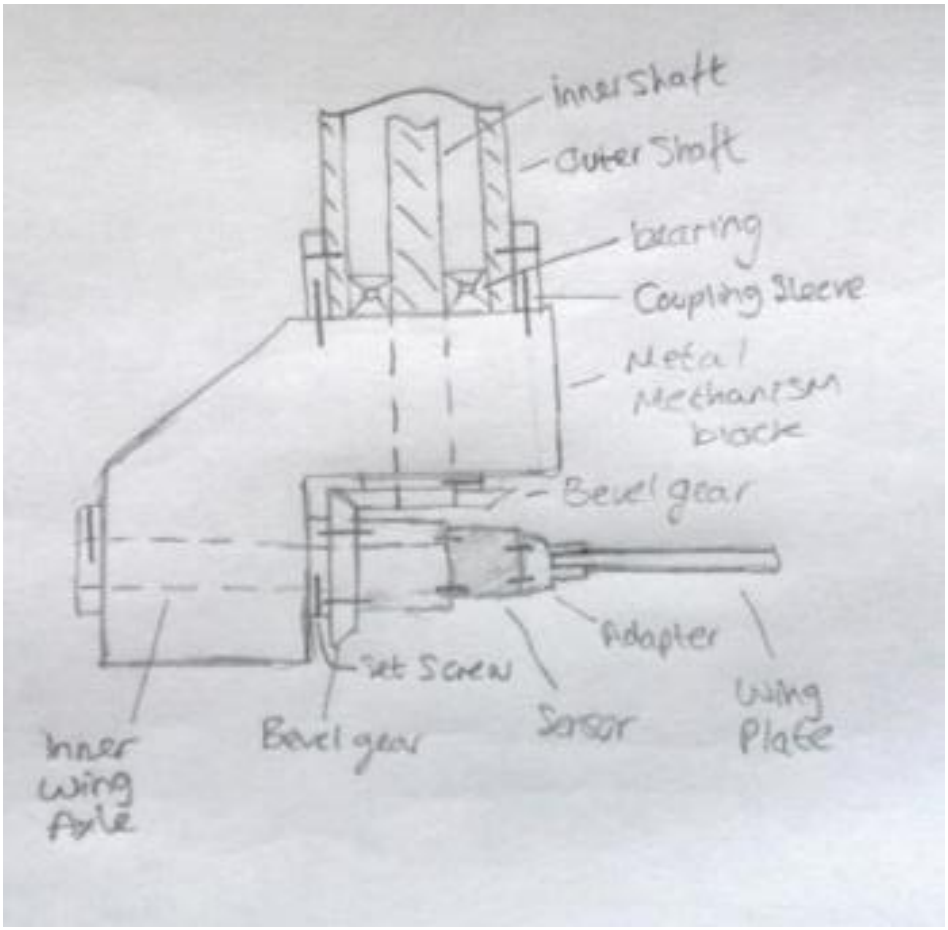

Figure 3.1: Initial design sketch of bevel gear sub-assembly

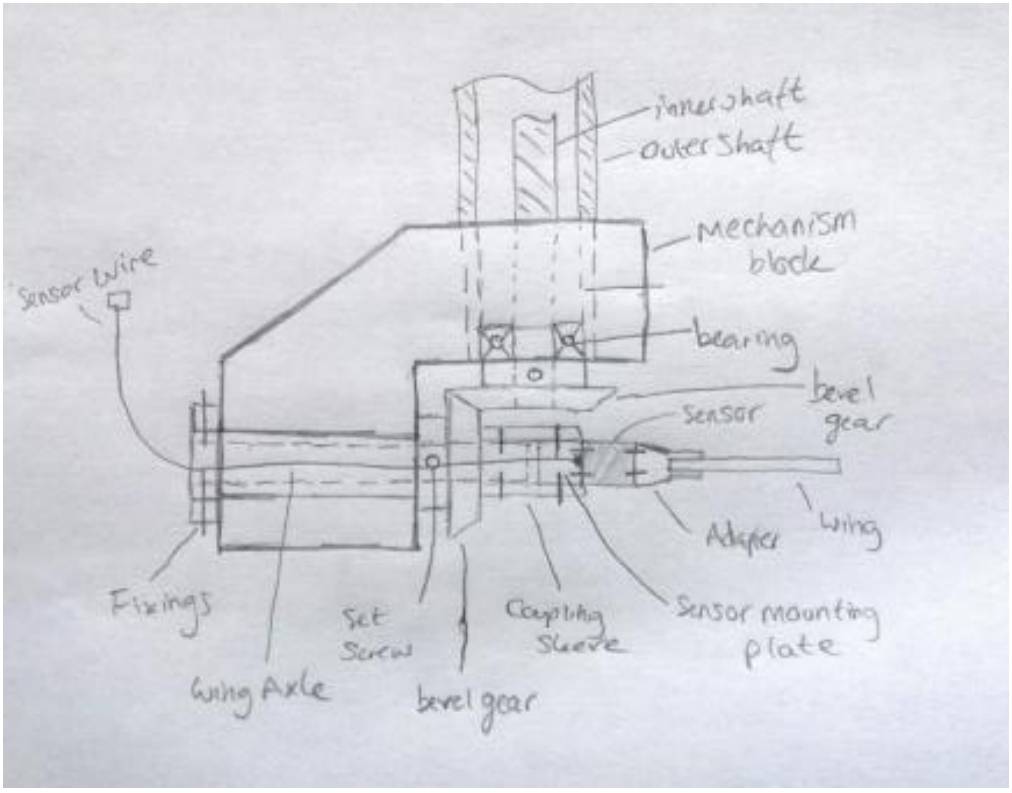

Figure 3.2: Detailed developed design sketch

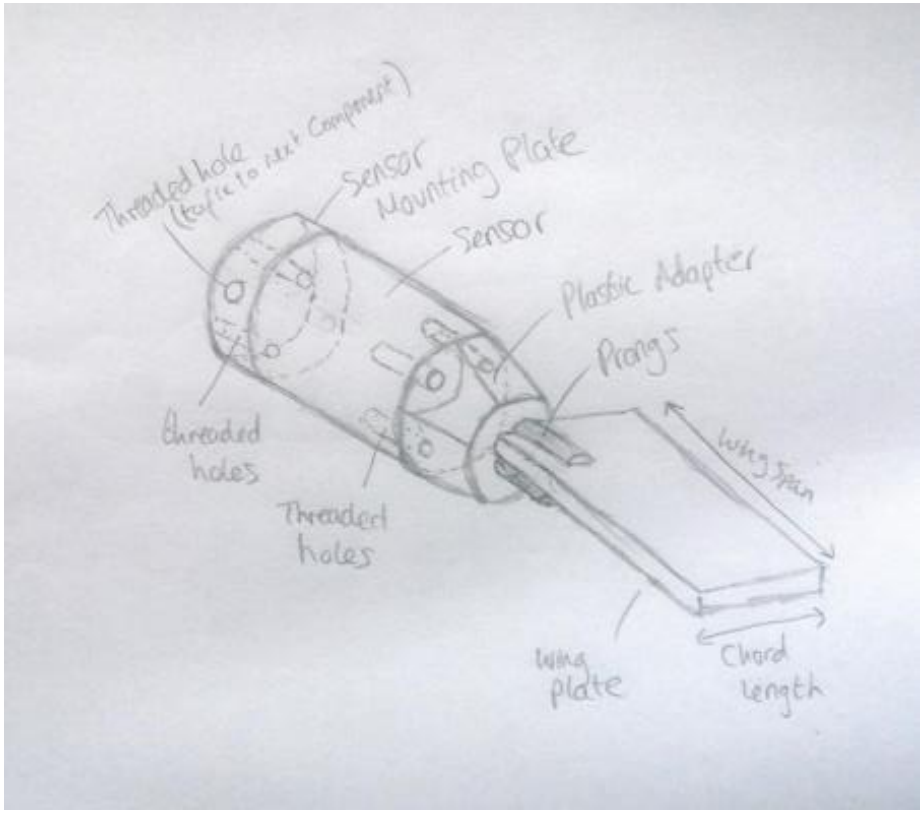

Figure 3.3: Sensor mounting strategy

Figures 3.1, .3.2 and 3.3 show the initial designs surrounding the mounting of the sensor, bevel gears and shaft inputs.

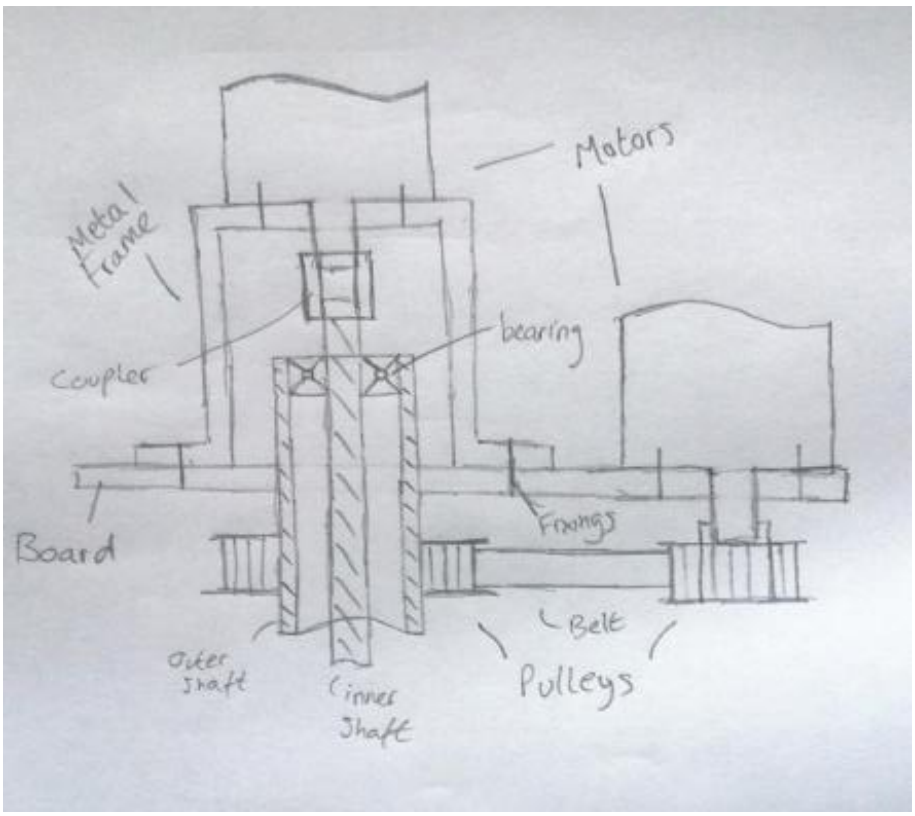

Figure 3.4: Initial sketch fixing stepper motor to board

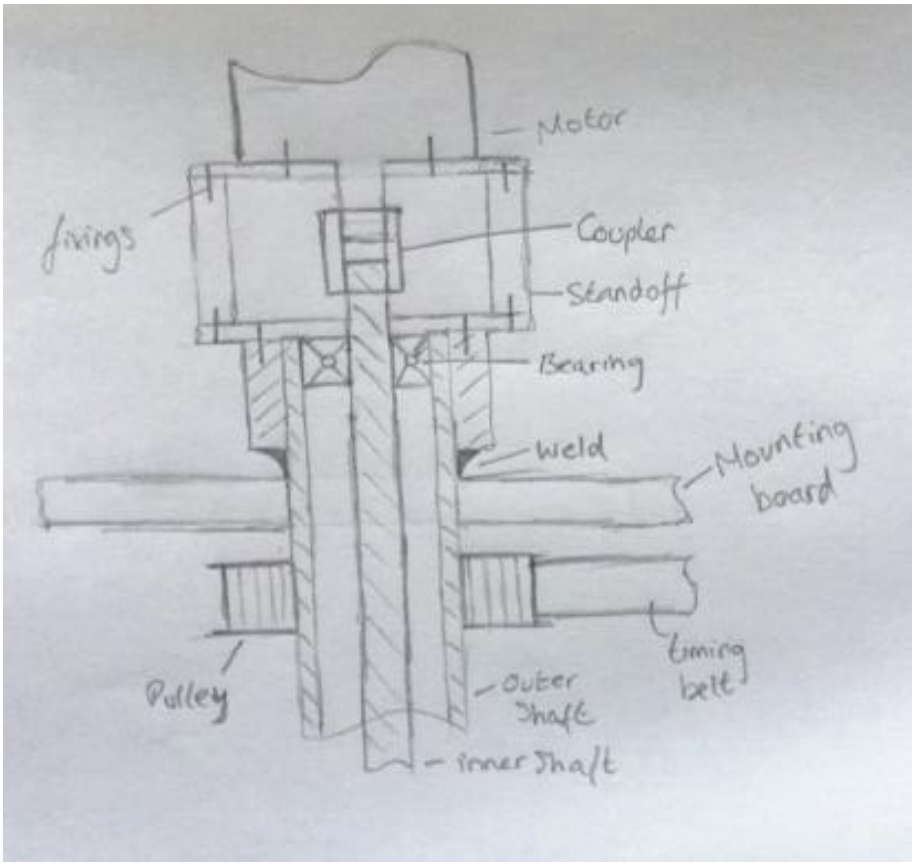

Figure 3.5: Initial sketch fixing stepper motor to outer shaft

Figures 3.4 and 3.5 show the possible solutions to the backlash issue where the stroke motion causes a change in pitch angle as one bevel gear rotates around another. Either the stepper motor is fixed to the board and programmed to rotate in sync with the stroke motion, or the stepper motor is mounted to the outer shaft as to rotate in unison.

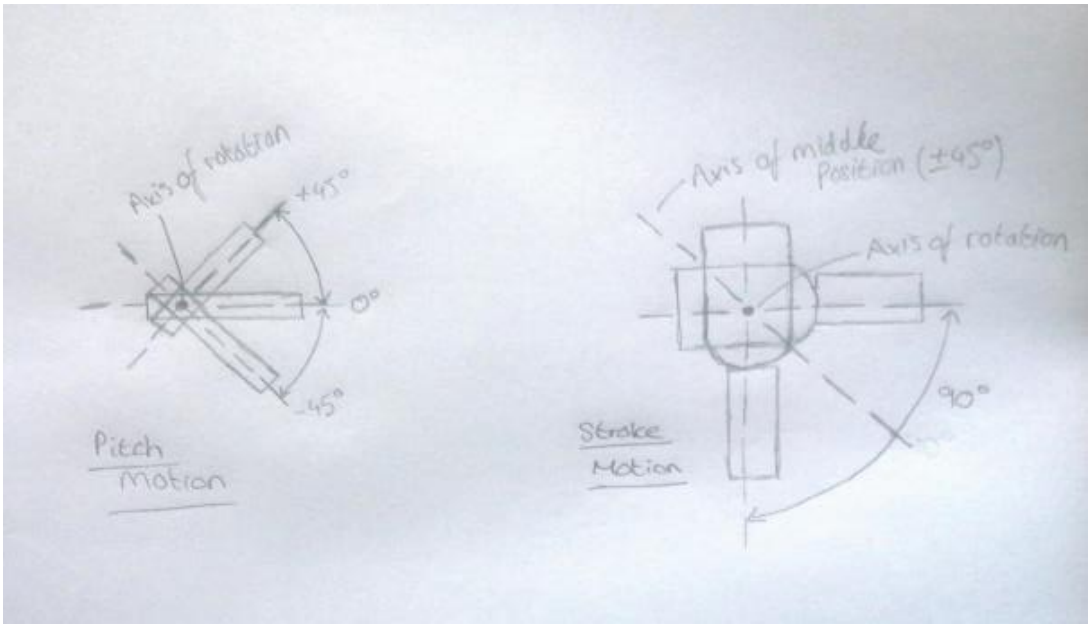

Figure 3.6: Target wing and stroke angle range

Figure 3.6 illustrates the range of positions we are aiming to achieve with the design with reference to a neutral position at an angle of 0°.

3.2. Design Fundamentals:

3.2.1 Design Overview:

The initial CAD designs of the two basic sub-assemblies are shown below. Figure 3.7 shows the motor and pulley systems that provide the mechanical input, whilst figure 3.8 shows the bevel gear system that transfers motion through to the wing.

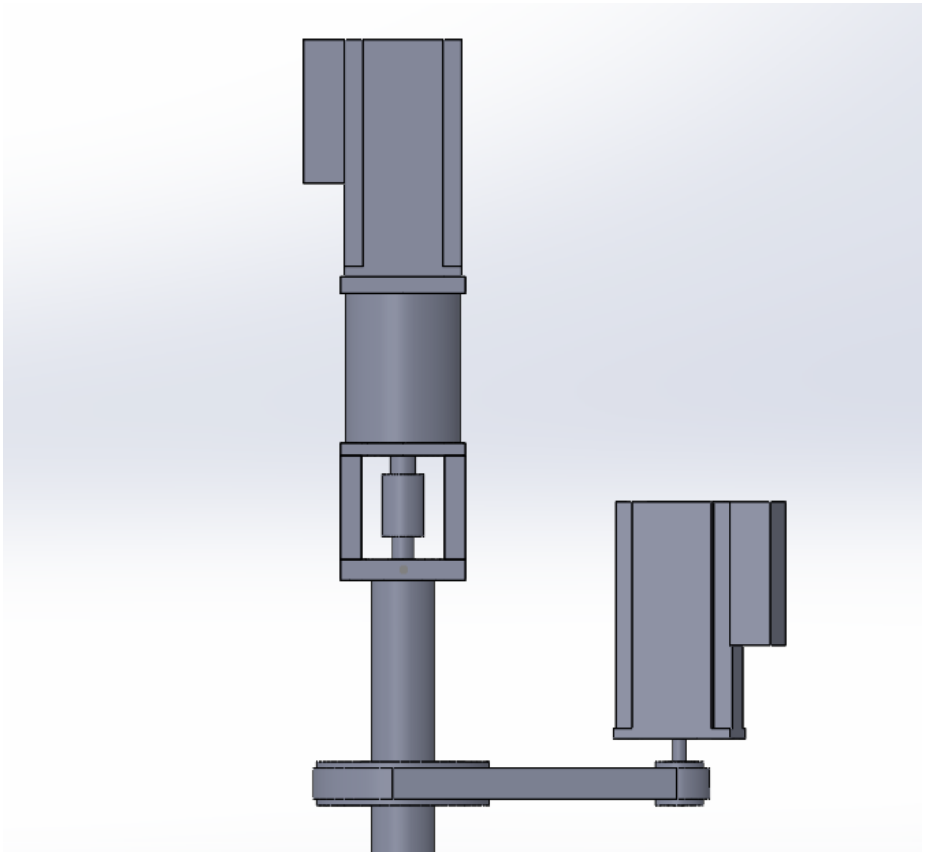

Figure 3.7: Motor and pulley system sub-assembly

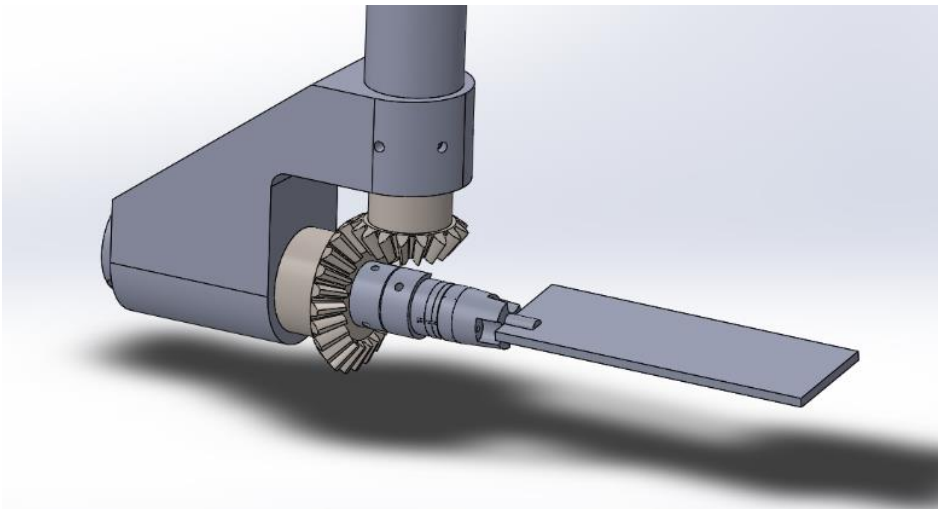

Figure 3.8: Bevel gear system sub-assembly

Both stepper motors have their outputs processed through a form of gearing that changes the speed, torque and output step resolution size. These provide great design flexibility to aid in providing sufficient torque or more desirable resolution sizing. The pulley system can convert the motor output into rotation of the outer shaft therefore changing the stroke angle. The second stepper motor instead uses an inner shaft and

bevel gears to actuate a change in wing pitch angle by changing the axis of rotation by 90°.

To reduce the effects of deflection on the inner shaft, a pair of deep groove ball bearings are used. These can be inserted at either end of the outer shaft ensuring alignment between the inner and outer shafts at either ends. The positioning of these bearings in the shaft are displayed in the sectional view in figure 3.9 and use a changing in shaft thickness as a shoulder to hold the bearings in position.

Figure 3.9: Assembly of Outer shaft, Inner shaft and alignment bearings

The length of the outer shaft was chosen at 0.6m which allows for ~0.5m of reach into the water tank. This allows the motors and signal converters to be mounted at distance from the water and create no risk of damage. This also aids in the mounting to the existing frames that are positioned above the tanks.

The initial design can then be developed further by creating a suitable mounting arrangement. This includes adding the main 12mm plywood mounting board accompanied with a flanged bearing. The flanged bearing is crucial to the design, as it is the most effective way to fix the outer shaft at a certain height whilst still permitting rotation. The board includes a series of slotted cut-outs to permit the fixing of the board to a mounting frame and also the pulley stepper motor onto the board. Figure 3.10 shows the produced board with attached bearing and motor.

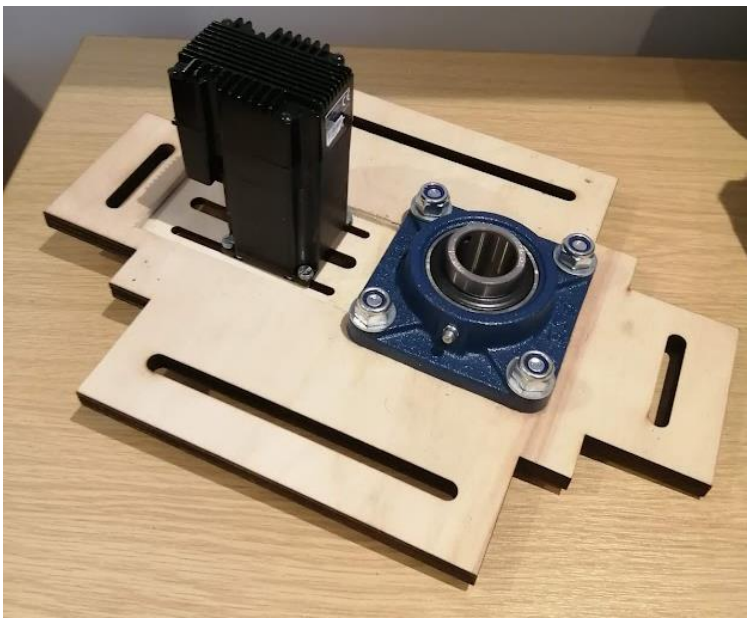

Figure 3.10: Image of manufactured mounting board

Implementing this completes the overall design and allows the creation of a final CAD overview. This finalised design can be seen in figure 3.11.

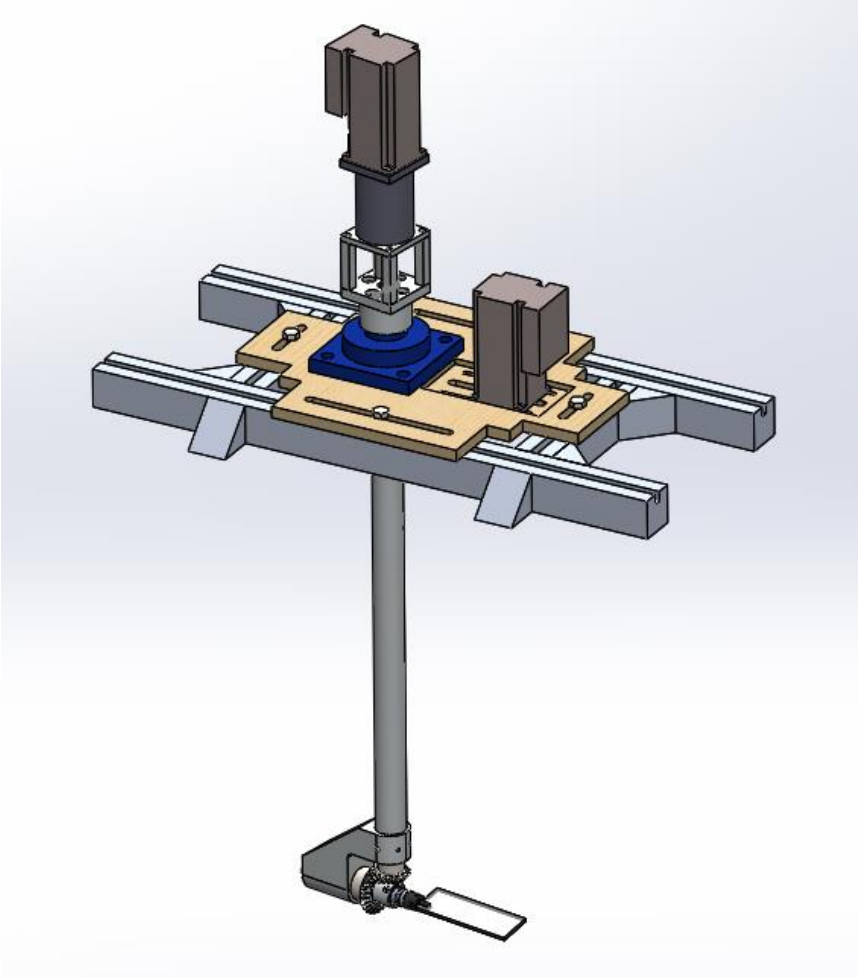

Figure 3.11: Final Apparatus design

The image also includes an aluminium extrusion frame that will then be fixed to the lab tank's frame. These lengths of extruded aluminium are linked together using right-angled brackets depicted above as triangular components. A visualisation of the apparatus positioned above the UOS static water tank is shown in figure 3.12.

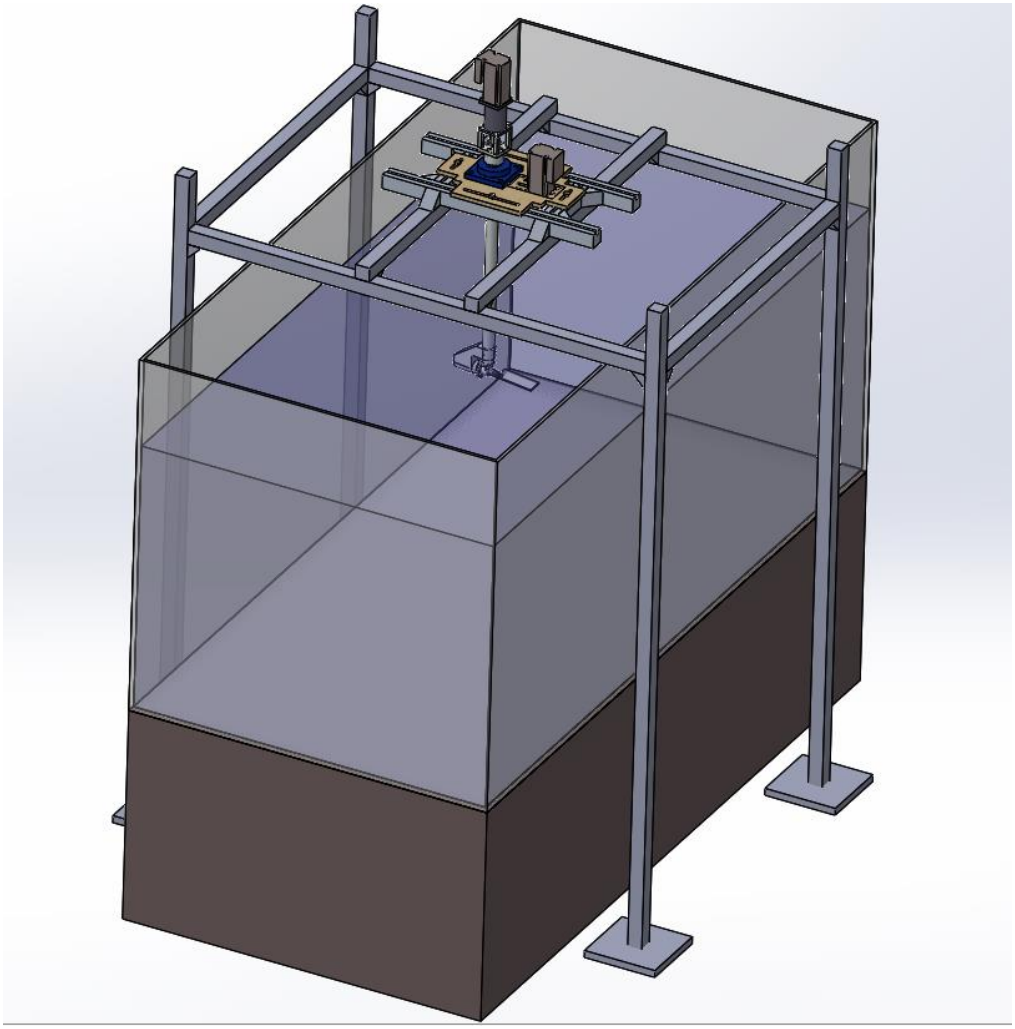

Figure 3.12: Flapping wing apparatus positioned on the water tank frame.

3.2.2. Power Transmission:

To explore how we can provide the required torque, we have to think about the two required features of the motion separately. To achieve the motion, we will start by needing to choose a motor, and after consideration outlined in Section 3.5.1 the chosen motor is the STM-23S-3RE which is rated with a torque of 1.41Nm [28]. If we then compare this to the required torque to perform the pitch and stroke motion, we know that the stroke exceeds that provided by the motor whilst the pitch falls dramatically below. This means that a gear system is required to be able to change the supplied torque and enable the experimentation. Using $T_{required}/T_{motor}$ = Gear ratio (GR), it can be said for the

stroke motion the torque is out by a factor/gear ratio of 4, whereas the pitch torque can be supplied by the motor.

During the design process, multiple gearing systems needed to be explored including bevel gears, spur gears and pulley systems. Comparing these methods is important to justify which method we proceed with whilst also weighing up against costing. Using bevel gears comes with a great increase in cost which is not justifiable for the stroke motion when compared to the alternate methods. Whilst during the literature review, we learned that pulley systems whilst simple can leave room for error if not properly taught. [12]

Eliminating bevel gears for the stroke motion, Table 3.1 compares the possible methods we could have employed to achieve the gear ratio of 4.

Transmission method:	Spur gear	HTD Pulley	Justification
Mounting method			Greater flexibility in mounting distance with belt length
Maintenance			The belt drive has greater maintenance however replacement of worn-out components is quick and simple
Durability			Belts wear out far before the gears obtain noticeable damage
Protection			Belt drives require no additives or protection for functionality
Vibration			Rubber belt provides greater absorption of vibration and disturbances
Efficiency			The gearings provide similar efficiencies, spur gears have slightly greater however not enough to stand them apart, also pulleys have no need for a keyway

Table 3.1: Spur gear vs. Toothed timing belt pulley

The chosen method of power transmission is the use of a high torque drive (HTD) timing belt and pulley set. This was the most suitable of the options for our purpose and our situation. This involves the factors of accuracy, manufacturing, assembly and budget. The pulley system comes in 4 components: a 48-tooth driven pulley, a 12-tooth driving pulley, a 425mm-long HTD belt and a locking bush (all shown in figure 3.13). The number of teeth on the pulleys decide the gear ratio, and therefore 48/12 = GR = 4.

Figure 3.13: Purchased HTD toothed pulley components

The sizing of these components can be used to diagrammatically show the mounting distance between pulley centres in figure 3.14. This distance effects the design of the mounting board and where the stepper motor would be positioned.

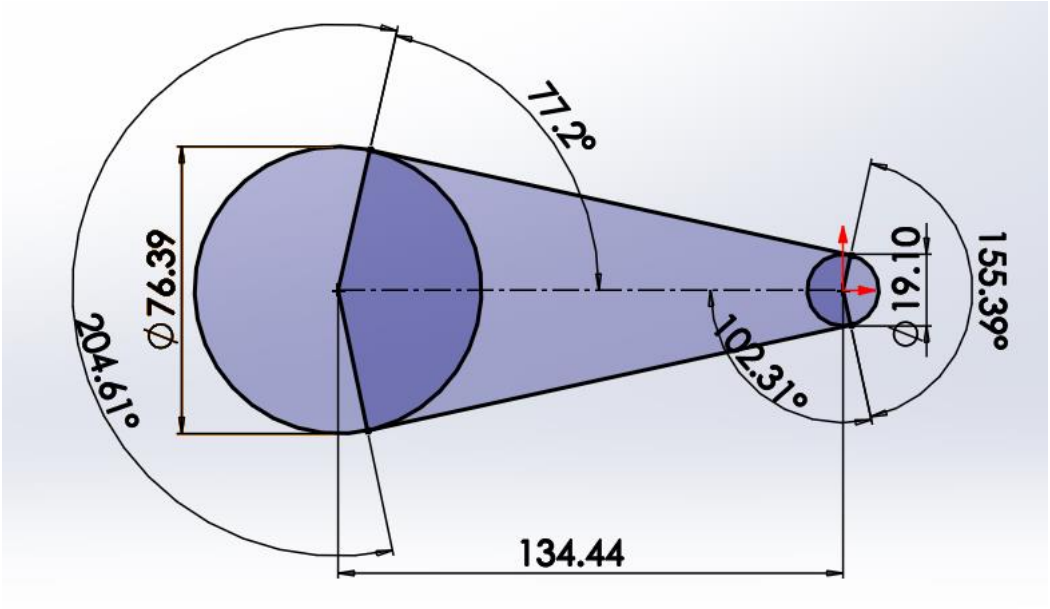

Figure 3.14: Diagram of pulley spacing, diameters and belt length

For the pitch motion there is no need to increase the torque, this does not mean the gear ratio will be irrelevant, there is instead value in trying to increase the resolution of the wing position. With the motor having a 1.8° resolution [28] and the target wing position range of ±45°, a finer degree in wing position is required. It was decided, the design will use a set of bevel gears to change the axis of rotation from the y-axis to the x-axis so by choosing an applicable gear ratio we can increase the accuracy of the resolution.

A set of steel bevel gears were found with a 1.5 GR, using a 16-tooth driving gear and 24-tooth driven gear (pictured in figure 3.15 below). This 1.5 GR then creates a 1.2° pitch angle resolution for the rig, which can be further improved with an planetary gearbox. The gears are ordered with set screws, and a 10mm (16-tooth) and 21mm (24-tooth) bore corresponding the design of the inner shaft and wing axle.

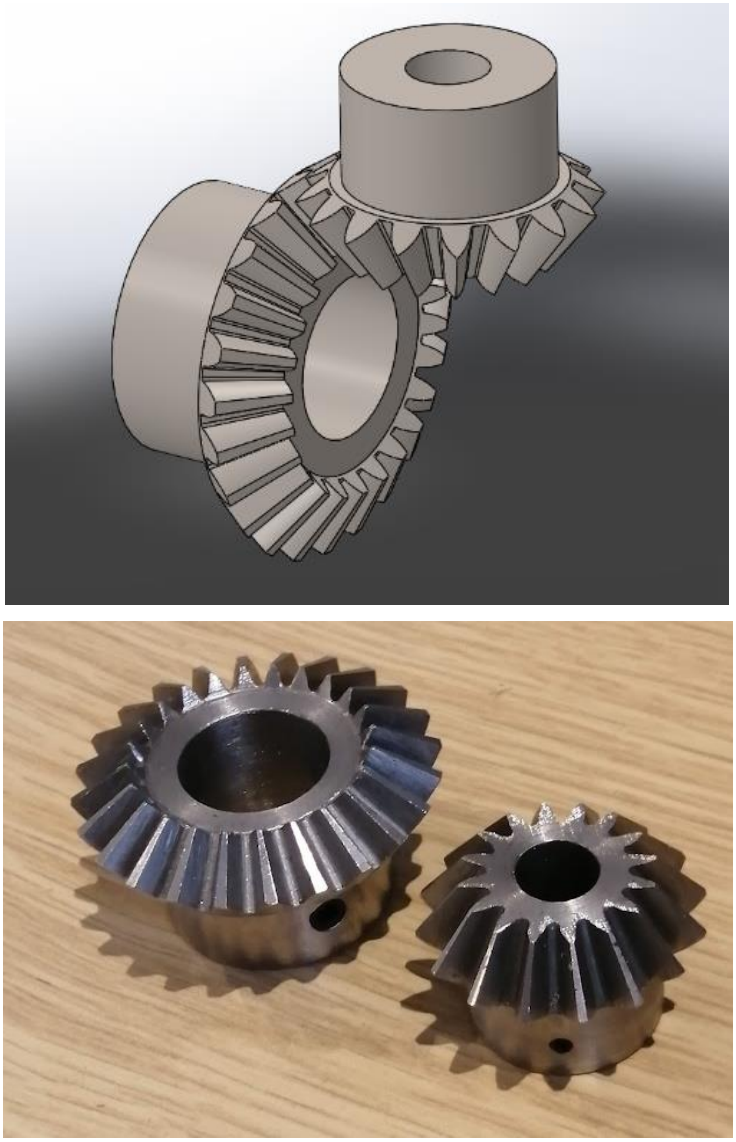

Figure 3.15: a) Steel bevel gear pair in Solidworks (top), Purchased bevel gears (bottom)

Using the gear manufacturer's provided mounting distances (base of one gear to centre of second gear) of 40mm and 37mm [29], it was possible to ensure these distances were properly implemented like shown below in figure 3.16.

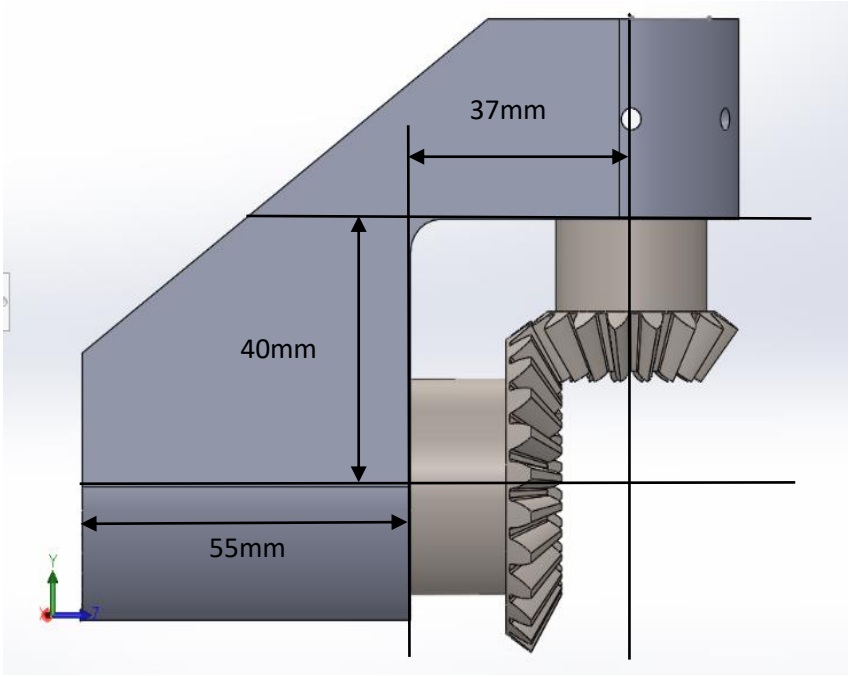

Figure 3.16: Mounting distances for the bevel gears

3.2.3. Wing, Sensor and Adapter:

The chosen wing model was the same as that found in the literature and that is a rectangular plate of chord 34mm and span of 107mm. The ATI Nano17 IP68 is a sensor model submergible in fresh water to a depth of 10 meters and has a force and torque resolution of 3.13mN and 0.0156Nmm respectively. [30] The sensor is available for me to use from the UOS and uses an arrangement of threaded holes for both mounting of the wing and to the apparatus. To therefore to fix the acrylic plate to the sensor, an adapter will need to be designed that fixes the two together.

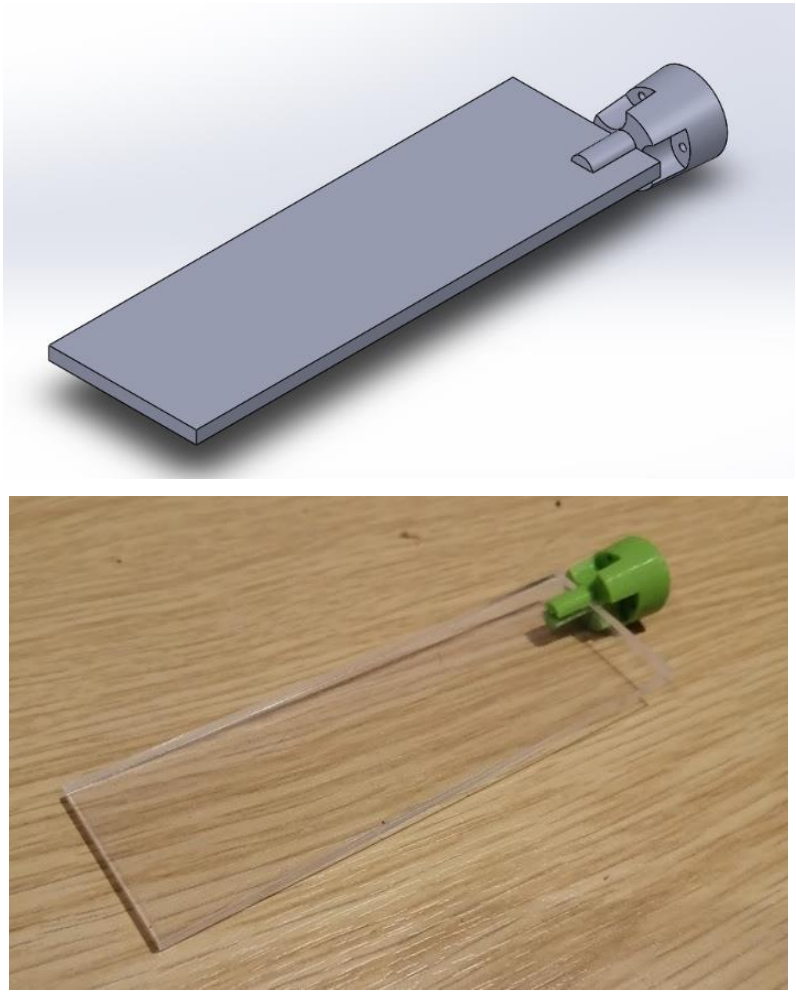

Figure 3.17: a) CAD of wing and adapter assembly (top), b) Manufactured adapter with acrylic wing (bottom)

Figure 3.17a) shows the design that will be implemented. Figure 3.17b) shows the manufactured adapter and how it holds the plate on either side with two prongs in a pressure fit that can be glued to create full security. The design of the prongs mean that they only protrude into the wing only 10mm and have a thickness of ~2mm as to not dramatically affect the flow over the wings and be a factor in the experimentation's results. Example flow over the wing can be modelled using software like Solidworks Flow Simulation, figure 3.18 shows an example flow path.

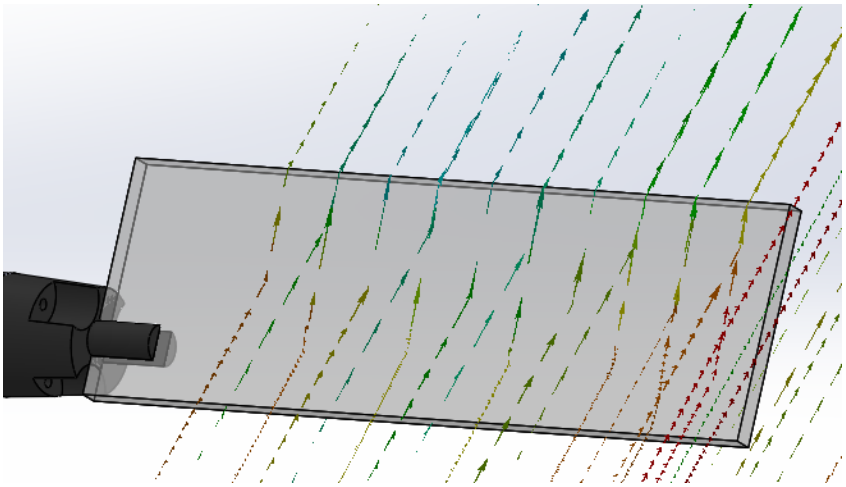

Figure 3.18: Flow visualisation over the wing

The problem the Nano17 sensor poses to the apparatus is the route the axially-exiting cable must take. A path must exist for the sensors wire to pass through otherwise the design will not work. To allow for this, the components have been designed to either allow for the sensor to pass through them with the cable following or use a cut channel for example the wing axle and the back plate that mounts the sensor. The back of the sensor and the wire can be seen from the rear of the apparatus as shown in figure 3.19.

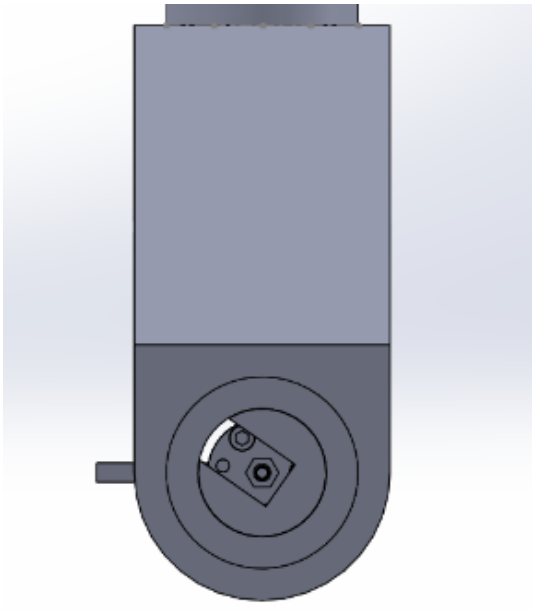

Figure 3.19: Nano17 sensor wiring route

3.2.4. Motion Mechanisms:

Both mechanisms are powered by the chosen stepper motor and controlled with a signal converter. The waveforms will be coded on a software like MATLAB and then uploaded to the motors causing the actuation. The software allows for a wide flexibility of

waveforms and programmable motions being able to control the motions amplitudes and frequencies.

3.2.4.1. Pitch Mechanism:

In the case of the pitch motion, the outputted motion will pass through an planetary gearbox reducing the resolution with a GR of 1:6 down to just 0.3°. This then travels the length of the inner shaft where it drives the bevel gear pair reducing the resolution value once more down to a final 0.2°. The overall GR from input to output is 1:9 and therefore to create the 90° change in α from -45° to +45°, the stepper motor needs to complete 810° of rotation (or 2.25 revolutions).

To continue the output from the 12mm gearbox shaft [31] to the 10mm inner shaft, a Ruland Jaw coupler is used. Shown in figure 3.20, the coupler is made of 3 pieces: two jaws and one rubber spacer. Each component is ordered separately and therefore compatibility must be checked.

Figure 3.20: Ruland jaw coupling [32]

A 12mm bore and 10mm bore set of jaws were selected with the corresponding 33mm diameter rubber coupling between. The jaws fix to the shafts by tightening the screw in the side of the jaw. This form of coupler has been chosen as it further helps the alignment of power output and flexes to ensure this. If the coupler experiences axial loading however, it will separate apart. To stop this, it is possible to further machine the coupler and use a fixing to hold the two jaws together.

Figure 3.21 shows 3 positions of the wing, these are 0, -45° and +45°. These angles correspond to the neutral position, and maximum and minimum angles of attacks.

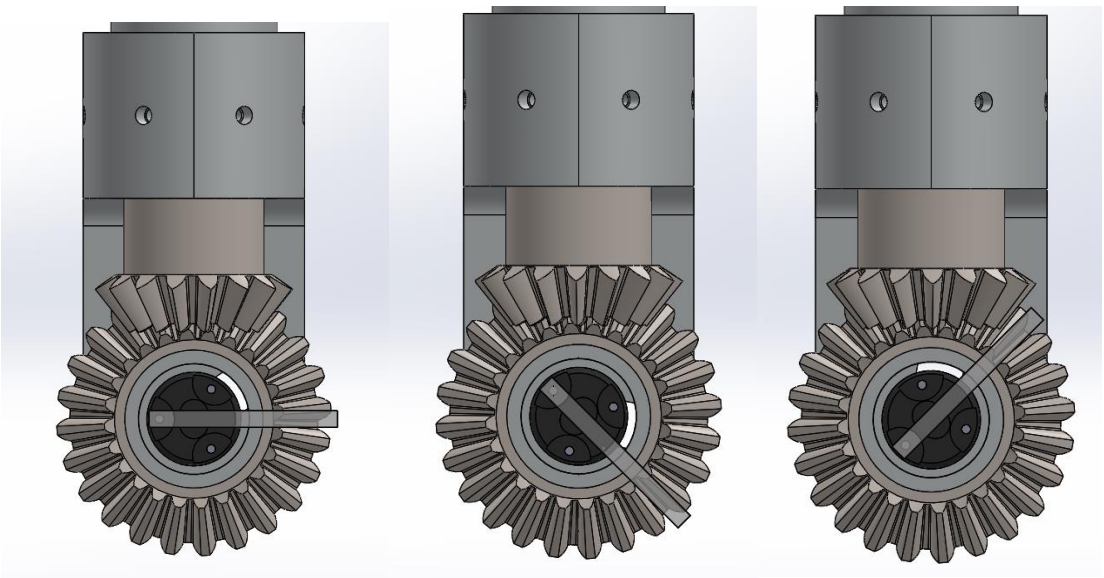

Figure 3.21: Apparatus at pitch angles: 0, -45° and +45°

These angles are shown clearer using a 2D drawing from the view of the wing tip in figure 3.22.

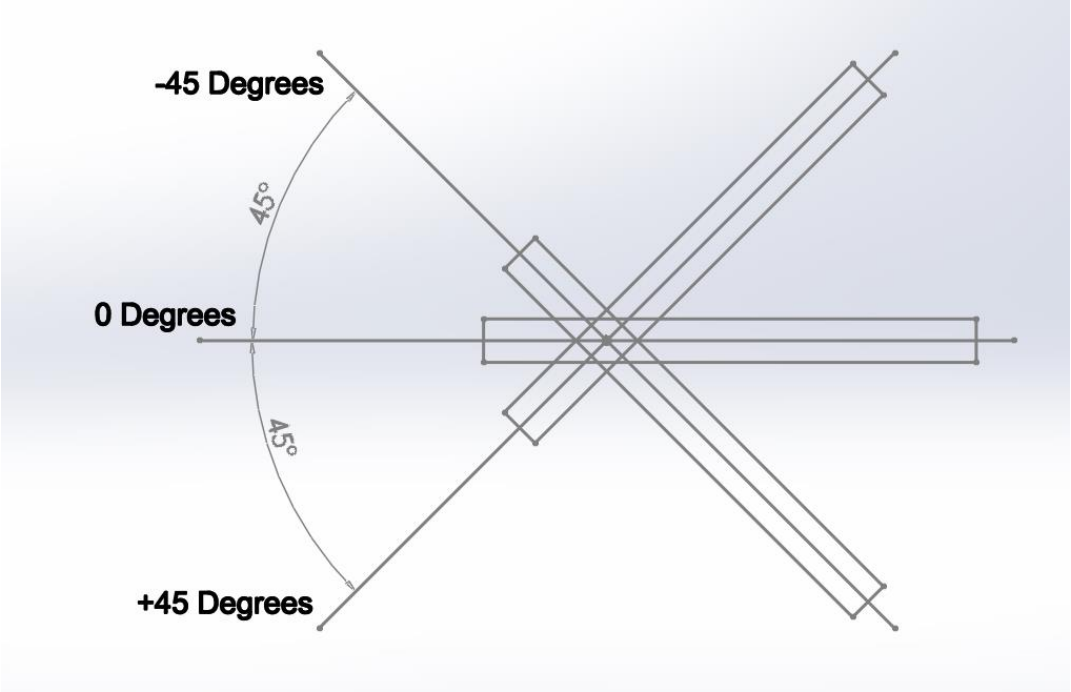

Figure 3.22: 2D drawing of pitch motion

3.2.4.2. Stroke Mechanism:

In the case of the stroke motion, the motor first rotates the small 12-toothed pulley, this then uses the timing belt to rotate the larger pulley and therefore also the outer shaft. The pulley gear ratio of 4 means that a total 5.64Nm torque acts on the outer shaft. This also means the stroke positions has a 0.45° positional resolution.

Figure 3.23 shows the full 90° sweeping range that will be employed in testing. The apparatus is capable of a sweep greater than 90° however this would start to cause issues with the sensor wire wrapping and stretching as it covers such a large motion.

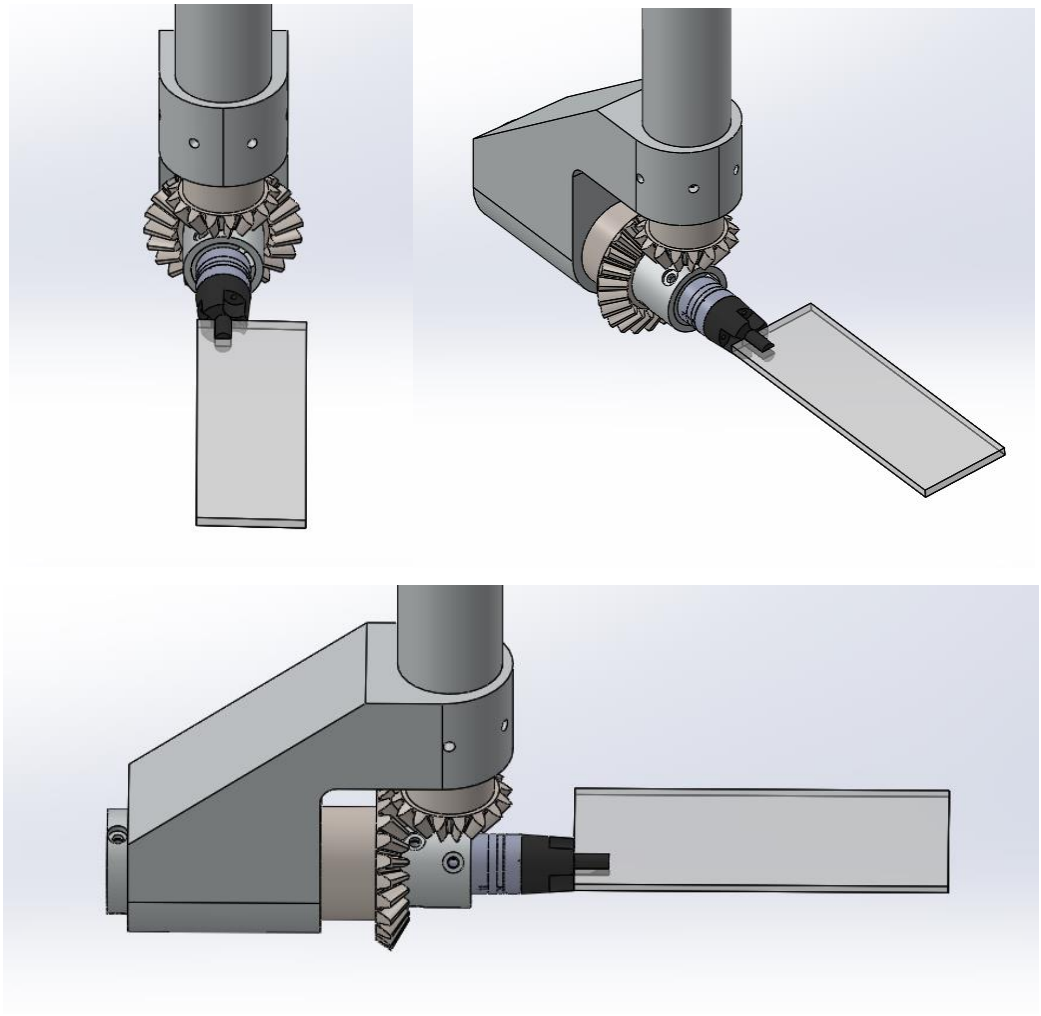

Figure 3.23: Apparatus at stroke positions: 0, 45° and 90°

These angles are once again shown clearer using a 2D drawing this time from above in figure 3.24.

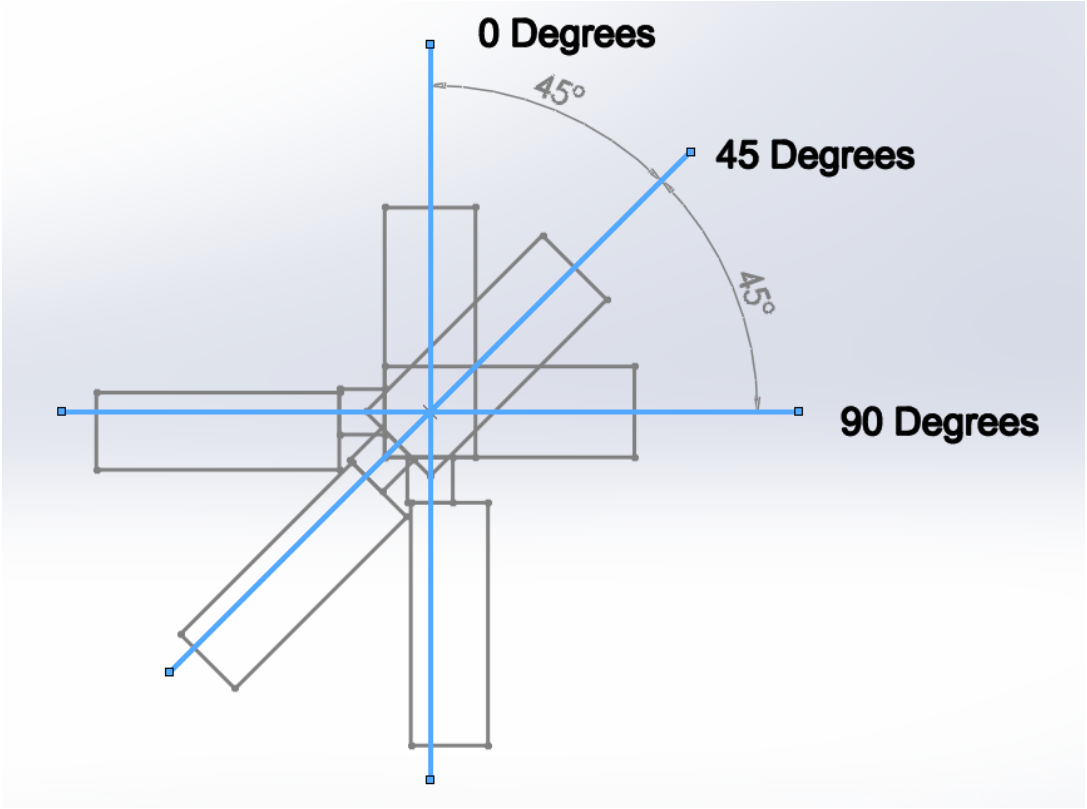

Figure 3.24: 2D drawing of stroke motion

3.3. Material Selection:

The choosing of materials involves a careful balance of mechanical properties and budgeting/availability. The ideal material for the set-up will have substantial strength compared to its weight. To allow for ease of assembly and lower resistive weights/forces, a reduced weight is optimal. The only components that are affected by serious loads are the inner and outer shafts. These are the components where strength will be required. If the material is not strong enough, the component will deform and fail. The property that will gives a good indication of failure is the material's yield strength.

Shown below in figure 3.25 is a comparison produced using GRANTA Edupack to create a comparison between yield strengths for a range of materials. The materials have been limited to predominantly plastics and metals that wont rust. This is because of the water environment of the testing.

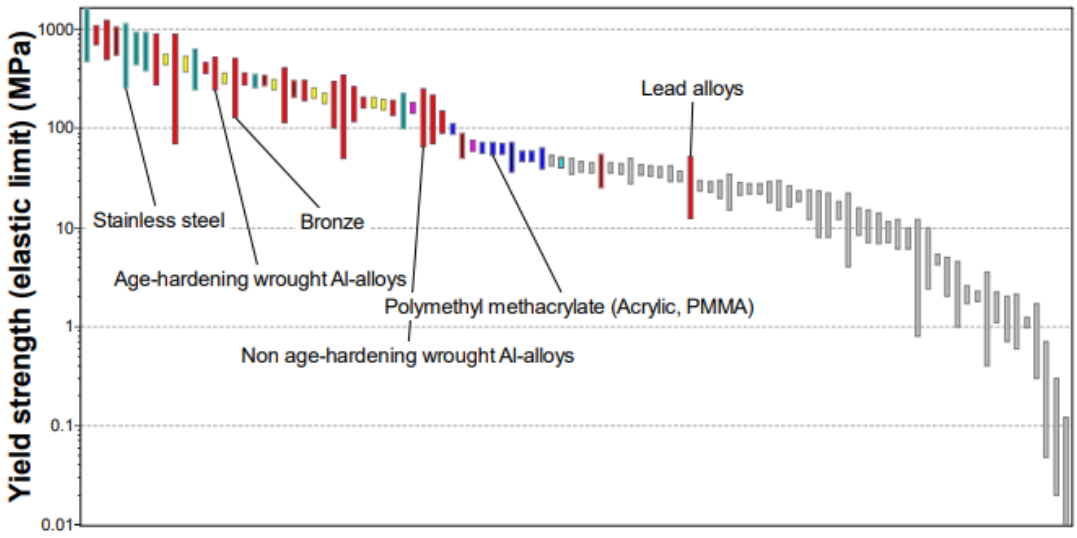

Figure 3.25: Yield strength against density for potential materials

Engineering design projects depend on a variety of inputs and one of the strong limitations is the project budgeting. After assessing the possible materials, only stainless steel and aluminium are reasonable choices. Both these materials are sufficiently strong enough and suitable for water-submersion without serious corroding which is the main priority for testing. Between aluminium and stainless steel, the main difference is their strengths. Stainless steel not only has a greater density (7900Kg/m^3 compared to 2700Kg/m^3 [33,34]) but also a greater Young's Modulus than aluminium (190GPa compared to 70GPa [33,34]), which means that it would be less impacted by the effects of vibration. However, due to these material properties, the apparatus would be heavier and the time and material costs are far greater. This means for our production we will have to use aluminium for the construction. This material is far softer and allows for quicker additional machining were tolerances not great enough and extra machining was required. 6082 T6 Aluminium is readily available inside the Engineering Design and Manufacturing Centre (EDMC) and is kept in constant stock.

The bevel gears are manufactured from EN8 mild steel, and therefore will require begin to rust over time from being submerged in water. This means the gears will require drying after use to slow down this process and eventually may need treatment or replacing. The material used for the wing plate is clear acrylic laser cut in the EDMC whilst the 3D printed adapter is produced from Polylactic acid (PLA). These are both cheap and easily accessible from the University.

3.4. Design Validation:

3.4.1. Design Capabilities and Customisation:

The design would theoretically allow for unimpeded rotation for a full 360° for both axis of movements however this is limited by the sensor's data/power cable. This cable could pose the problem of not only twisting the cable but also tangling or pulling out of its power pack if it was to be stretched too far. The cable could theoretically be clipped onto the outer shaft to stop such free motion in the water however this would not completely solve the issue especially the cable twisting. Because of this the angle of attack should not be used past ±90°, whilst the stroke motion should only be used to a maximum 180° sweep.

The design has been made in a way that allows for simple customisation and changes that allows for a variety of future experimentation and improvements.

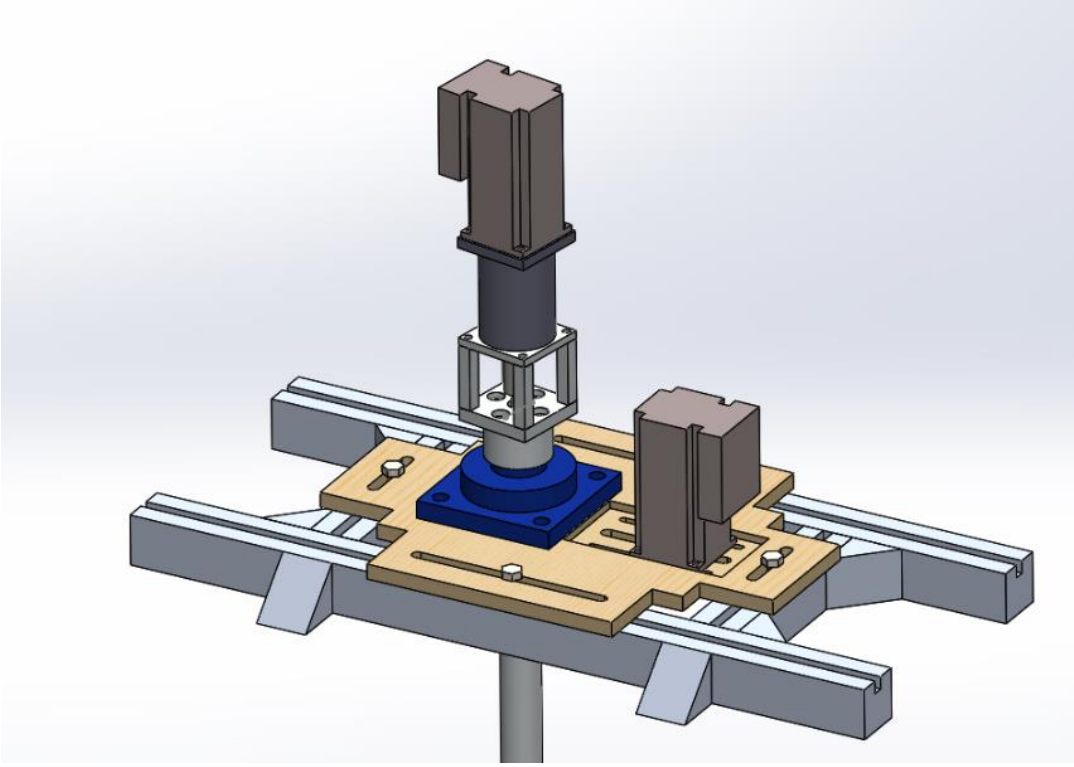

Figure 3.26: Apparatus section above the tank

The final mounting apparatus shown in figure 3.26 uses simple connections and a modular design to separate the fixings attributed to each component. In the future a different stepper motor with higher torque or finer resolution may want to be used, and as the motor and the gearbox is fixed to a customised plate, a new plate could be designed and swapped in to implement this change without effecting the rest of the set-up. As for the pulley system motor, redesigning and creating a new plywood board would be simple and cheap to create.

If the apparatus was to be used in flow greater than planned for, the required torque through the pulley would be greater. If this was to be the case, a new pulley could be ordered, compatible with the current locking bush, but with a greater number of teeth. This would increase the GR and possibly solve this issue. This is only applicable up until the maximum pulley size compatible with the bush.

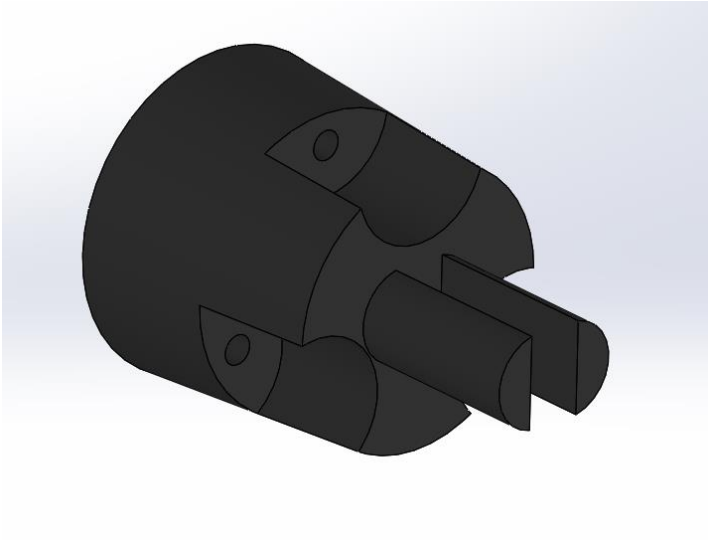

Figure 3.27: 3D printed adapter from wing to sensor

The PLA adapter pictured in figure 3.27 couples the sensor to the rectangular plate wing we chose at the start of this project. There is a lot of possible research with different wing shapes, their aspect ratio but also the effect of the wing flexibility. When this round of research is required, another adapter can be quickly 3D printed and attached onto the sensor. All the adapter needs are three M2 clearance holes corresponding to the sensors interface. The pronged design should be capable of holding a wide variety of AR as long as the lengths do not become too great. If the plate thickness was also to be changed, the spacing between the prongs would also require changing. However, for a flexible wing an alternative to the prongs would need to be designed, likely involving two rods the flexible material would be secured on.

3.4.2. Torque Requirements:

Now that the core of the set-up is designed, the expected torque of using the rig in the RWT can be calculated. As mentioned earlier, this will allow us to choose what driving torque we need to provide for the rig to function. The area used for modelling the resistive forces has been found from our current design. For the stroke motion, the side-on area of the sub-assembly is related to the force experienced in flow as shown in the equation written below.

$$F = \frac{1}{2} C_D \rho A {U_{inf}}^2$$

Equation 2: Force exerted by flowing fluid

$$U_{inf} = V_{inf} + 2\pi f R$$

Equation 3: Equivalent flow speed for object oscillating in fluid flow

First using Eq(3) an equivalent flow speed can be found to be used to calculate the torque. Modelling in the recirculating water tank will be done at V_{inf} 0.3m/s and at an apparatus frequency of 1Hz. By combining this with the largest distances to the axes of rotation, R_{stroke} = 140mm (0.14m) and R_{pitch} = 25.5mm (0.0255m), a calculation can be done to find U_{inf}. These calculations are shown below:

$$U_{inf,stroke} = 0.3 + 2\pi \times 1 \times 0.14 = \ 1.18 m/s$$

$$U_{inf,pitch} = 0.3 + 2\pi \times 1 \times 0.0255 = \ 0.46 m/s$$

Using C_D = ~2 [35], these values can be used for the force calculation outlined in Eq(2). These calculations are shown below (with ρ = 1000kg/m^3):

$$F_{stroke} = \frac{1}{2} \times 2 \times 1000 \times (0.241 \times 0.9) \times 1.18^2 \ = 30.2N$$

$$F_{pitch} = \frac{1}{2} \times 2 \times 1000 \times (0.034 \times 0.107) \times 0.46^2 = 0.770N$$

Then by using T = F*R, the maximum torque can finally be found. This yields the results T_{stroke} = 4.228Nm and T_{pitch} = 0.196Nm. The torque involved in the pitch motion is minimal and even if this underestimates the required torque, a stepper motor is likely to be able to drive it. The stroke torque overestimates the area involved in the motion greatly, it should then follow that if this torque can be provided, the apparatus will be capable of full function.

3.4.3. Design Resolution:

The resolution of the design has been decided by the motors, gearbox and gears. The final resolution of the wing angle of attack is 0.2° whilst the stroke position resolution is 0.45°.

Figure 3.28: Image of planetary gearbox

The motors each have 1.8° resolution and then after a 1:6 gearbox (example shown in figure 3.28) and 1:1.5 bevel gear pair give the 0.2° whilst the 1:4 pulley gear ratio gives the 0.45°. These resolutions are sufficient for our experimentation and allows for fine control over the wing position over time. However, this could be further improved with a change of components if ever required. By changing out the motors or gearbox the resolution could changed until satisfactory, however this requires the purchasing of components far beyond our budget. The motor we used has a Nema23 shape type and specific shaft size, if the available gearbox was not compatible with this shape, then either one would require purchasing or the design would need to proceed without a gearbox and a much poorer resolution of 1.2°. Therefore, it was fortunate there was a compatible gearbox readily available to be used. The motors mount flush to the flange ending of the gearbox using four M5 screws and nuts. The arrangement of these components can be seen in figure 3.29.

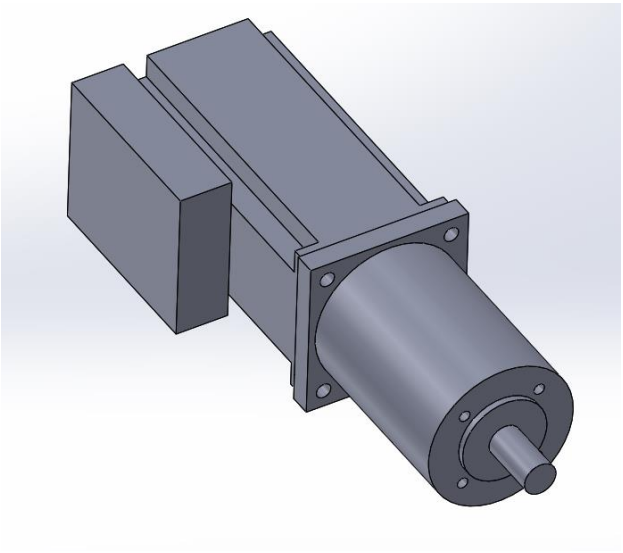

Figure 3.29: Nema23 stepper motor shape mounted to compatible gearbox

In addition to the positioning resolution, as stated earlier in Section 3.2.3, the sensor also has a force and torque measuring resolution of 3.13mN and 0.0156Nmm respectively. They are the fine degrees that our results will be accurate to and so this is very important to be aware of. If our resolution was not sufficiently small enough, the data gained would be useless as there would be far less detail and variation.

3.4.4. FEA Analysis:

The functionality of the project has been thoroughly validated and rationalised, however no assessment has been made for structural stability. A simplified Finite Element Analysis (FEA) model of the outer shaft would show the forces experienced during testing. The analysis would involve assigning appropriate constraints (like the flange bearing only permitting rotational motion and no axial deflection) and modelling the 4.228Nm torque experienced by the stroke motion.

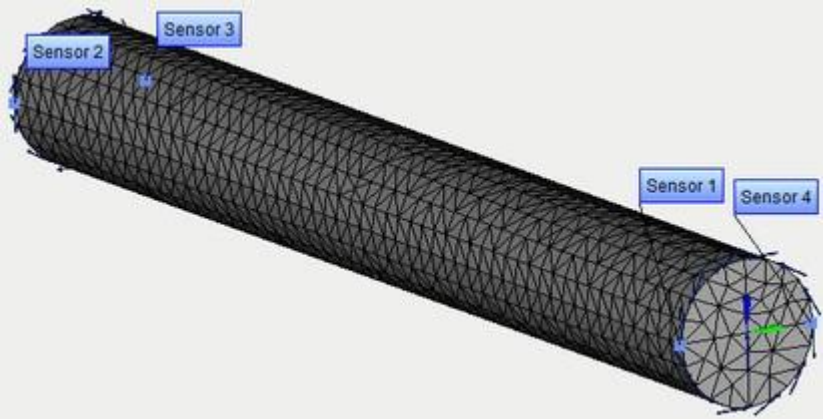

Figure 3.30: Example FEA mesh on a cylindrical shaft [36]

Figure 3.30 shows an example mesh on the cylindrical shaft, the number of elements will affect both the model accuracy and processing time. The model can have an appropriate mesh sizing applied and solved for shear forces throughout the length. The results of this modelling can be compared to the materials yield strength to prove if the material would shear or not and what safety factor is in effect for the rig. Further modelling to show shaft deflection could also be performed as this could affect the accuracy of the modelling motion position.

3.5. Motor Control and Data Recording:

3.5.1. Motor Selection

To deliver the motion we have designed for, two motors need to be used, each controlling their own axis of the motion. For our experimentation, the prioritised aspects for the motors, are the torque, step size (resolution) and costing. Servo and stepper

motors are the two most common types, both are suitable for application and therefore a choice needs to be made on which to employ. Whilst servomotors typically are more efficient and capable of a greater torque, stepper motors tend to have a stronger holding torque. The holding torque is an important factor as the motor actuating the pitching motion will use this to ensure the inner shaft rotates in sync with the outer. Stepper motors are capable of producing the required torque and with a great availability of models accessible through the UOS, this was the motor type that was chosen.

The STM-23S-3RE stepper motor was chosen due to availability within the university. Appendix B displays the engineering drawings for this motor, with key information like the mounting information and output shaft dimensions clearly defined. Table 3.2 lists some of the key technical values related to the motor including the power requirements that will need to be supplied.

STM-23S-3RE Stepper Motor	
Specification	Value
Supply Voltage	12-70 VDC
Applicable Control type(s)	Step + Directional Control, Serial Commands
Step size	1.8°
Additional step functions	Half step and Microstep
Holding Torque	1.48Nm
Nominal Torque	1.41Nm
Weight	1.19kg
Shaft diameter	6.35mm
Mounting strategy	4 x 5.5mm holes

Table 3.2: Stepper motor technical data

3.5.2. Software Programming

The chosen motor will be programmed by inputting serial commands written into a software like MATLAB. To allow the motor to interpret the information coming from the software it must be translated using a USB-to-Serial Converter. Imaged below in Figure 3.31, is the ES-U-3001-M model that will be used.

Figure 3.31: ES-U-3001-M USB-to-Serial data converter [37]

Experimentation will require two units (one for each motor), the converter uses a simple cable (similar to that used on Arduino R3 boards) to receive data from a computer whilst 6 pins are used to transfer the data to the stepper motor. Out of these 6 pins, only 5 will be used, and will uses lengths of male-to-female wires to connect to the motors. Table 3.3 lists the connections from the converter to the motor.

Converter Pin	Corresponding Stepper Motor pin
TxD-	RxD-
TxD+	RxD+
RxD-	TxD-
RxD+	TxD+
GND	GND

Table 3.3: Converter to Motor wire connections

3.5.3. Sensor Data Reading

As mentioned earlier in Section 3.2.3, the sensor we had chosen to use is the ATI Nano17 IP68 model. The model is fitted with an axial cable shown in appendix C that exits the rear of the sensor and is plugged into an Interface Power Supply (IFPS) box. This box will connect into its power supply (can be wall mounted supplies depending on the model) and also use a 26-pin female DAQ port to allow for data collection. An example IFPS is shown in figure 3.31 with labelled DAQ port.

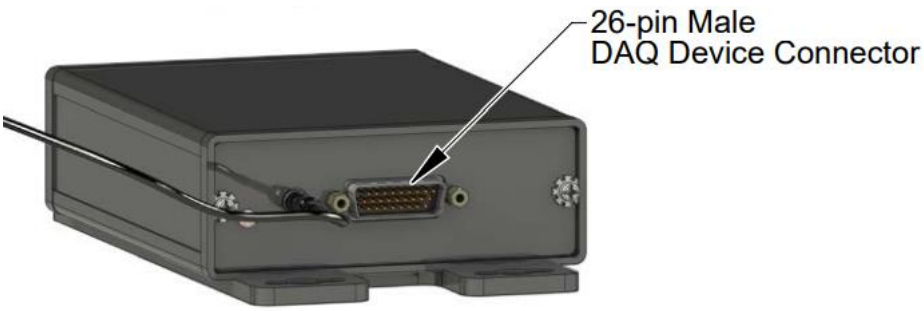

Figure 3.32: IFPS Box [38]

The sensor produces transducer data that is then interpretated by a DAQ device. The device converts the incoming data into force and torque readings experienced by the sensor. These values can then be either saved to a data card or transferred via USB straight to a computer. Post-processing and analysis of these results can be performed computationally after that.

4. Manufacturing:

This section will outline any manufacturing steps and changes that were made compared to the theoretical final design. The engineering drawings for the final design components manufactured in the EDMC are shown in Appendix D. For this project we were provided with financial budget of £100 and an additional budget of 21 hours of EDMC technician time. Any problems and changes made to adhere to this budget have been stated in the following sub-section.

4.1 Budgeting changes

Now the final design is in hand it is important to draft up a costing for each component in the design. This has been done and is shown in table 4.1 and 4.2.

Part	Material	Supplier/Source	Quantity	Total Cost
12mm Mounting board	Plywood	UOS	1	£0
3mm clear wing plate	Acrylic	UOS	1	£0
3D printed wing adapter	PLA	UOS	1	£0.10
Nano17 Back plate (20mm bar)	Aluminium	UOS EDMC	1	£0.50
Axle-to-back plate coupler	Aluminium	UOS EDMC	1	£0.65
Wing axle (20mm bar)	Aluminium	UOS EDMC	1	£0.50
Retention ring/end cap	Aluminium	UOS EDMC	1	£0.95
Outer shaft	Aluminium	UOS EDMC	1	£26.06
Inner shaft	Aluminium	UOS EDMC	1	£1.75
Outer shaft-to-plate coupling sleeve	Aluminium	UOS EDMC	1	£1.85
Shaft end plate	Aluminium	UOS EDMC	1	£1.25
Gearbox mounting plate	Aluminium	UOS EDMC	1	£0.80
Mechanism block	Aluminium	UOS EDMC	1	£52.44
			Total	£86.85

Table 4.1: Costing of Manufactured components

Part	Material	Supplier/Source	Quantity	Total Cost
Deep groove ball bearing	Steel	RS Components	2	£6.26
M6 60mm Standoff (pack of 5)	Zinc coated steel	RS Components	1	£11.78
12-tooth pulley	Steel	Simply Bearings LTD	1	£10.24
48-tooth pulley	Steel	Simply Bearings LTD	1	£27.05
Pulley locking bush	Steel	Simply Bearings LTD	1	£7.07
HTD Pulley timing belt	Rubber	Simply Bearings LTD	1	£8.54
Bevel Gears	Steel EN8	Bolton Engineering Products	1	£95.48
Flange Bearing	Cast iron	RS Components	1	£18.14
STM-23S-3RE Stepper motor	Metal casing	UOS/Applied Motion Products	2	£0
USB to Serial Converter	Metal casing	UOS/Connective Peripherals	2	£0
1:6 Planetary Gearbox	Steel	UOS/Motion Control Products LTD	1	£0
Ruland Jaw 12mm	Aluminium	UOS/RS Components	1	£0
Ruland Jaw 10mm	Aluminium	UOS/RS Components	1	£0
33mm Ruland Jaw spacer material	Polyurethane	UOS/RS Components	1	£0
M6 bolts	Steel	UOS	12	£0
M5 machine screws and nuts	Steel	UOS	4	£0
M3 machine screws	Steel	UOS	12	£0
M2 machine screws	Steel	UOS	6	£0
ATI Nano17 IP68 Sensor	Stainless steel	UOS/ATI Industrial Automation	1	£0
			Total	£184.56

Table 4.2: Costing of purchased components

Some of the components are stated to read £0 and free of charge. This is due the component being available for use from previous projects or are just not produced from materials the University charges for. For the EDMC to produce the rig's components completely from stainless steel would have required 32.5 hours of technician time. This is why aluminium was chosen to produce the apparatus. However even from aluminium, the manufacturing time would still have been too great. To work around this, I would be required to perform my own additional machining. This is far easier working with the softer aluminium and so this is a suitable solution to the problem. The components the

EDMC produce will use hole sizes suitable for additional tapping post-production. I can then tap the threads into these holes and also implement a countersink when necessary. Simple components like the inner shaft and standoffs were removed from EDMC processing. This is because I could purchase existing female-to-female threaded 60mm standoffs (shown in figure 4.1) instead and I could cut the 10mm diameter bar (inner shaft) to length myself.

Figure 4.1: Four M6 60mm long hexagonal Standoffs

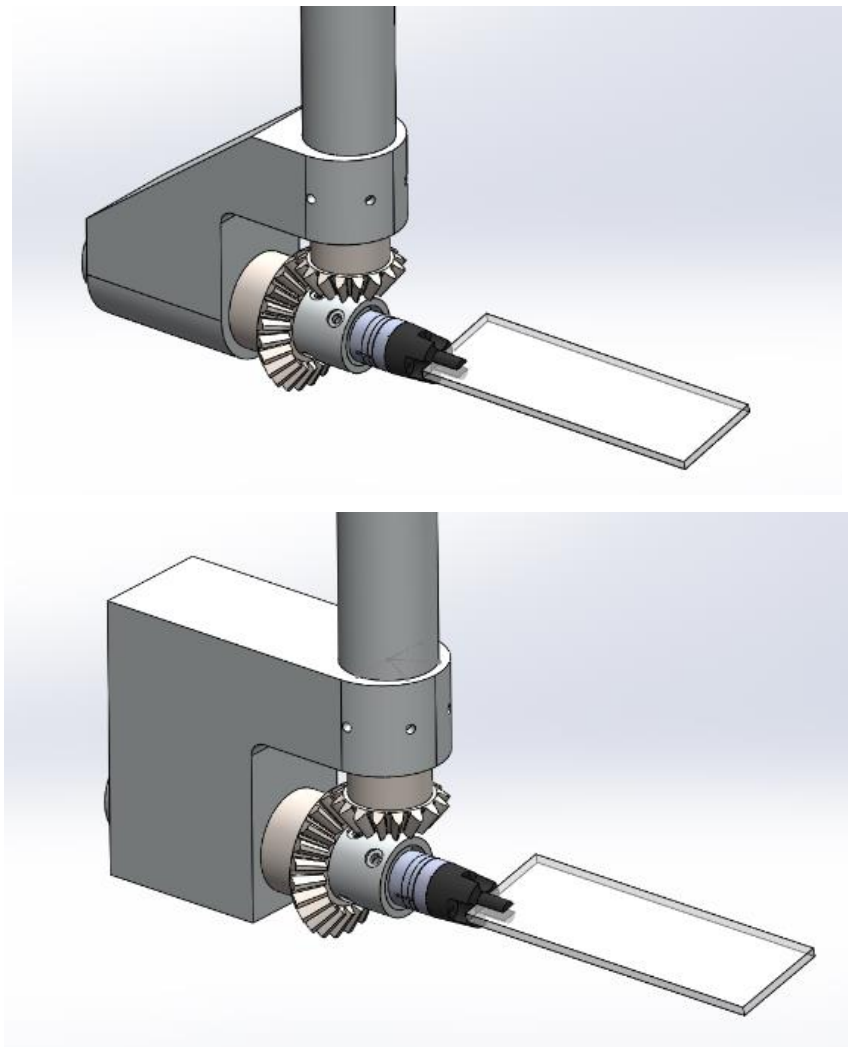

Figure 4.2: a) initial proposed design (top), b) manufactured design (bottom)

Despite this, the machining hours would still remain too great if the design was not changed. The desired design could not be produced and to meet budget restrictions, the mechanism block was produced to a far less streamline and lightweight design. Shown in contrast between figure 4.2 a) and b), it is seen that the cut along the back of the mechanism block and the 20mm fillet on the bottom have been removed to meet budget and fall to 20 hours of technician time. The milling of this component used too many EDMC and there was no other choice but to make this call. Fortunately, the second curved fillet on the block was not needed to be removed, this would be severely problematic as it is a fixing point for assembly and must not be removed.

Unfortunately, this could impact the experimental results as this will create greater disturbance to any water flow, however fortunately it will not stop the apparatus from functioning. Due to the overestimation in area of the required torque, the manufactured design is still capable of full motion and will be fully operational.

The last manufacturing change I had to implement is the addition of a set screw to the smaller pulley, depicted in figure 4.3 below.

Figure 4.3: Image of driving pulley [39]

The pulley comes with a pilot bore, this can then be machined out to 6.35mm. However, relying on a friction fit is not suitable for power transmission and therefore instead it requires the addition of a set screw which permits for up to a more general 6.5mm bore and guaranteed transmission. The issue with this is where to add the set screw, there is two options in locations. The set screw can be drilled into the tooth area of the pulley, but this may compromise drive effectiveness, or it could be located in a small area of excess material at the neck of the pulley. This area is 5.5mm wide and just allows for an M! or M2 set screw to be fitted. This should be sufficient to pin to the flat face of the stepper motor drive shaft.

4.2. Outer shaft

The outer shaft required specific machining for the design to work. Due to availability the only sizes of bearings that could accompany the 10mm inner shaft were 26mm OD. The outer shaft has an inner diameter (ID) of 26mm and therefore at either end the shaft required an 8mm deep thickness reduction from 3mm to 2mm. This can be shown with a detailed and section view onto the outer shaft. This view is shown in Figure 4.4.

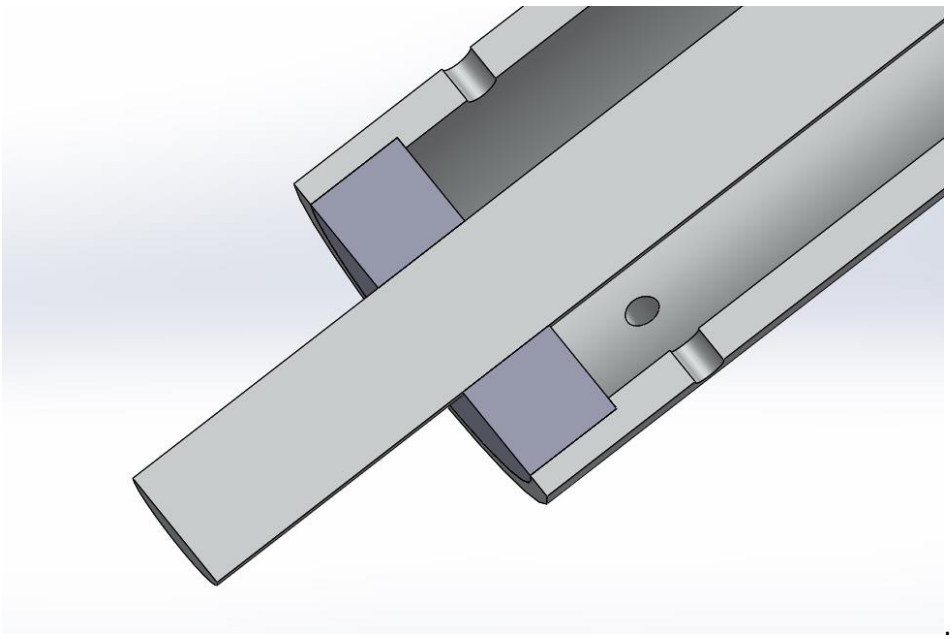

Figure 4.4: Section view of bearing arrangement

4.3. Overall Mechanism assembly

The steps required for successful assembly have been briefly outlined in Appendix E. These steps ensure the sensor is successfully installed, the gears interact properly and the set-up is mounted securely. The order of assembly is very important to have due to the components only fitting together in a certain order and sometimes requires performing multiple steps simultaneously. Creating a design that assembled was one of the most complex problems to overcome through this project, as the sizing of components had to be carefully thought out to allow clearance space but also fairly tight fittings to stop large levels of vibration. 1mm clearances and fitting spacing was decided as appropriate and used repeatedly across the design.

In the final stages of manufacturing, an error had been noticed with the sensor that was design for. The IP68 variation of the Nano17 does not have a 17mm diameter like the other models. Instead, a large 20.1mm diameter is used. To allow for assembly and allow the sensor to pass through the bores of other components, components had to be taken to the EDMC and rebored to a large 21mm instead of the original 20.1mm that was used. In addition, a new back plate was design and manufactured in the EDMC that was compatible with the mounting interface of the correct sensor.

4.4. Mounting

Possibly the key component in the mounting of the rig, is the flange bearing. This bearing allows for the design to be held in place at a pre-chosen height using a pair of two set screws. The bearing holds the rig but also permits for the outer shaft to rotate, which is crucial for the function of the stroke motion. Other alternatives like low-friction bushes

and shoulders were investigated but not implemented. The chosen bearing is illustrated in figure 4.5 and depicts the four interfacing bolt holes that secure it.

Figure 4.5: 4 Bolt flange bearing [40]

Following the selection of this component, a mounting board was design to allow for its fixing.

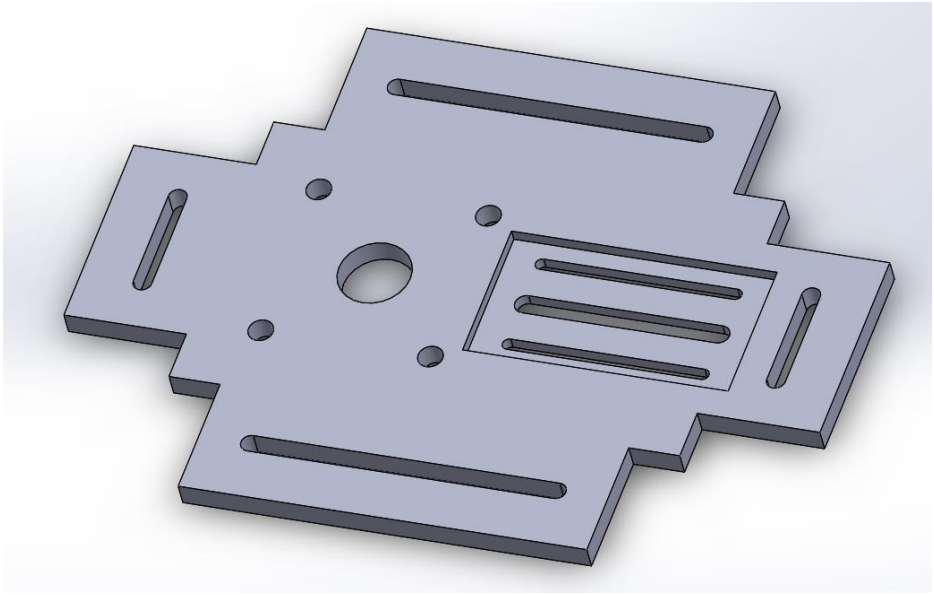

Figure 4.6: Mounting Plywood board

From figure 4.6 it can be seen that the board has been designed with corresponding holes for the flange bearing, slots and reduced thickness for the motor mounting and finally, slots for the frame fixing. The frame slots are 9mm wide along the outside edges of the board and allow for M8 bolts to fix through with washers into M8 inserts in T-slots extrusions.

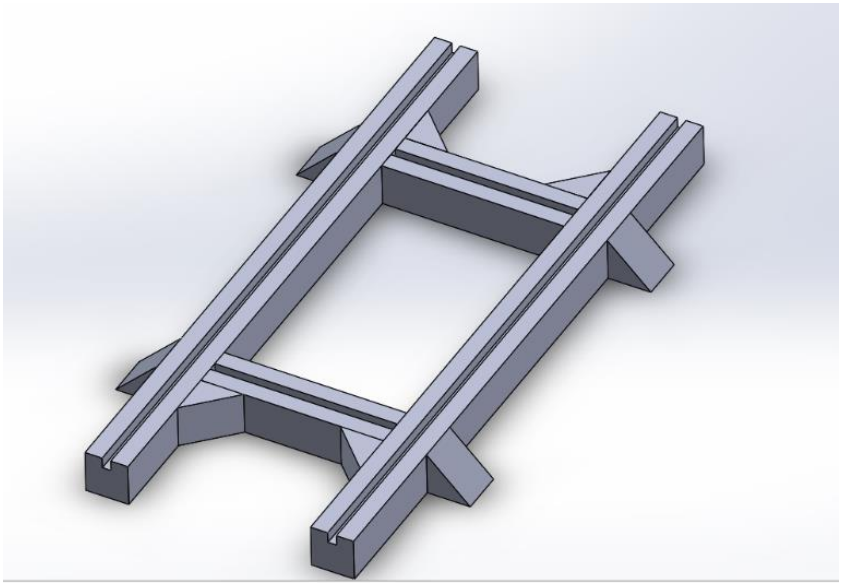

Figure 4.7: T-slot aluminium framing arrangement

Figure 4.7 shows the arrangement of framing that will allow the board to fix to. This can then be held together and bolted to the existing framing above the tanks using right-angled brackets (depicted as triangular components). The depicted grooves show where the M8 threaded inserts will be added to bolt into. The final bolted mounting assembly is shown below in figure 4.8.

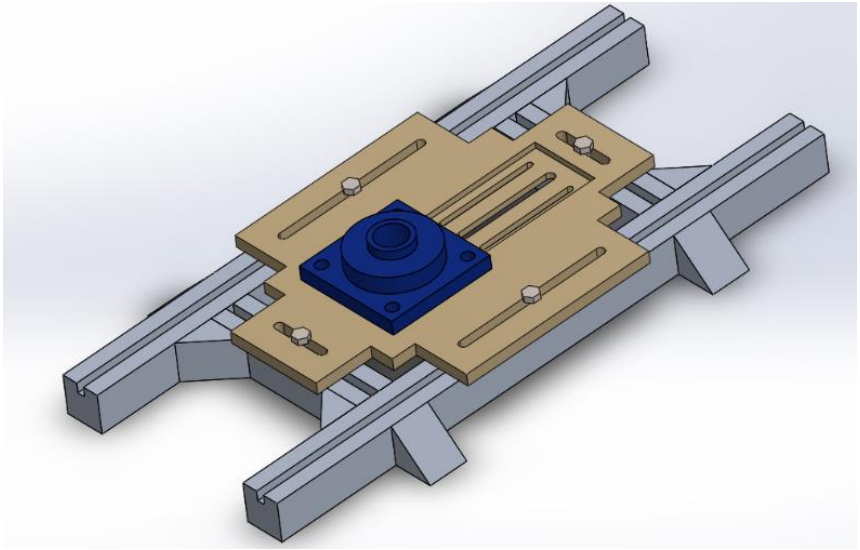

Figure 4.8: Final mounting assembly

4.5. Electronics

Using the available Electronic Workshop facilities on campus, wiring of appropriate length could be cut and prepared. By soldering together, the long cut lengths of wires to shorter existing wires with the necessary female pin connectors, the connection between motor and signal converters can be produced. For safety purposes, these solder joints are covered in heat shrink to insulate the joints. The power wiring for the stepper motors

is produced with the same methodology, however differing with connector types. The power connector into the motor uses additional screws to fix the connection to the motor and prevent it from pulling loose. On the other end of this wire is a connector that will plug into the 5V laboratory power supply.

The power supplies, IFPS and DAQ are all provided by the UOS Boldrewood Campus. This equipment is held in the laboratories and can be taken out for use at the time of experimentation. A quick risk assessment reveals that the main issue with electronic equipment is the proximity to water. Waterproofing the entire rig would be a long and expensive process. Alternatively, the rig has been carefully designed and positioned so the motors stay a safe distance from the water surface. The experimentation does not involve great speeds or water disturbance and therefore should not be presented with the risk of splashes, however if this turned out not to be the case, a splash guard (acrylic sheet) could be mounted to completely eliminate this risk.

5. Conclusion:

The design process of this experimental set-up has been a long and methodical process, constantly adhering to restrictions and budgeting challenges. Whilst drawing a great deal of inspiration from an existing design, there was still a large number of design issues to work around. Whilst this report has briefly covered the design requirements of each component and some of the thought process behind them, it does not cover the repeated iterative process of change that was needed to create a fully working design. Due to the dependency of neighbouring components, there were many occasions where the design required full remodelling due to new design inputs and decisions.

To conclude, the design of the rig has yielded an arrangement that meets its initial aims by allowing for the measurement and calculation of torque and power coefficients that can be used in further studies to influence the plausibility of using the hydrofoiling method in winged UAAV systems. The final design can be summarised as an aluminium apparatus capable of delivering rotation in two axes to create a sinusoidal waveform at the wing tip within 0.2° and 0.45° positional accuracy. The set-up uses stepper motors programmed with signal converters to create a sinusoidal wave form output at the wing. This motion is then to be performed in a laboratory environment in pre-chosen conditions, and measurements can be taken from the Nano17 sensor.

The results from this testing will allow for power, lift and drag coefficients at separate positions along the motion to be calculated. This study then allows for further experimentation to idealise these coefficients and make the most efficient motion with the greatest thrust production. This is the motion that would then be implemented into the future robotic drone designs.

6. Future work and Experimentation:

6.1. Mechanism improvements

Due to budgeting and timing constraint, there is still far more work to do to achieve useful results and implement possible design improvements. The improvements will allow for decreased drag and therefore less interference with the water environment and results. As stated in section 4.1, the design was changed for manufacturing and therefore the first improvements would revolve around reversing these design changes and streamlining the set-up once more.

6.2. Motor and gearbox alternatives

Following this, the design could be changed to shed weight and increase positional resolution. There are three ways for the design's resolution to be made finer. Firstly, a gearbox with a greater gear ratio can be used, however this will increase the overall apparatus weight and height. Secondly, a different stepper motor could be used with a lighter weight and finer step sizing. And lastly and most suitably, investigate the use of the motor's half-step and micro-stepping functions. The motors micro-steps allow for less than 1.8° movement and this then means the gearbox can be removed from the design reducing weight. The motors weigh 1.19kg each [28] and so being able to not remove the further weight from the gearbox is an appealing possibility. The gearbox also has a height of 71mm [31] and being able to reduce the overall height of the design further reduces the effects of vibration. Seeing as the motor will be the source of the vibration this is a very effective improvement. The overall height of the design stands at 920mm, this is separated into 578mm below the plywood mounting board and 330mm above. With the removal of the gearbox the height above the board would drop 22% and overall length would be reduced by 8%. If this change was to happen and the gearbox was to be removed, a new Ruland jaw would need to be ordered with a 6mm size to fix directly to the motor instead of the gearbox shaft.

6.3. Bearing/Bush Discussion

Another change that could improve the design would be to use further bearings or bushes to reduce the friction acting on the wing axle. Currently the wing axle rotates inside the mechanism block with a 0.5mm clearance, this will involve resisting frictional forces whereas if the axle instead rotated in bearings or low-friction bushes this will be reduced. Although this would improve the efficiency of the design, a bearing with 20mm ID would have a 32mm OD. This would require a far greater bore in the mechanism block and lead to far more material waste, the additional costing of machining this bore and purchasing these bearings was not justifiable for the current stage of my project. The

mechanism block is also only 40mm wide leaving just 4mm thickness of material on either side. Whilst aluminium would be sufficiently strong under this thickness, it is an unnecessary risk to take.

6.4. Experimentation and Modelling

The experimentation that has been planned with this equipment has been outlined in Section 2.4. The methodology and potential uses for the results were also discussed, and the environments the rig was to be used in were also stated. Further analysis is required for the design before testing, this is because there has yet to be a structural assessment made on the response of the outer shaft under the 4.228Nm load that will be experienced. Although the material properties and thickness show almost certain structural strength, the task of an FEA analysis is relatively quick and simple and will be greatly beneficial for peace of mind.

7. References:

[1] - C. Roh and M. Gharib, “Honeybees use their wings for water surface locomotion,” *Proceedings of the National Academy of Sciences*, vol. 116, no. 49, pp. 24446–24451, Nov. 2019, doi: https://doi.org/10.1073/pnas.1908857116.

[2] – Becker, Florian. (2009). Variational Correlation and Decomposition Methods for Particle Image Velocimetry. (accessed May 17, 2023).

[3] - D. L. Altshuler, W. B. Dickson, J. T. Vance, S. P. Roberts, and M. H. Dickinson, “Short-amplitude high-frequency wing strokes determine the aerodynamics of honeybee flight,” *Proceedings of the National Academy of Sciences*, vol. 102, no. 50, pp. 18213–18218, Dec. 2005, doi: https://doi.org/10.1073/pnas.0506590102.

[4] - G. E. STRATTON, R. B. SUTER, and P. R. MILLER, “Evolution of water surface locomotion by spiders: a comparative approach,” *Biological Journal of the Linnean Society*, vol. 81, no. 1, pp. 63–78, Jan. 2004, doi: https://doi.org/10.1111/j.1095-8312.2004.00269.x.

[5] - L. Zhao, Q. Huang, X. Deng, and S. P. Sane, “Aerodynamic effects of flexibility in flapping wings,” *Journal of The Royal Society Interface*, vol. 7, no. 44, pp. 485–497, Aug. 2009, doi: https://doi.org/10.1098/rsif.2009.0200.

[6] – A. Gehrke, G. Guyon-Crozier, and K. Mulleners, “Genetic Algorithm Based Optimization of Wing Rotation in Hover,” *Fluids*, vol. 3, no. 3, p. 59, Aug. 2018, doi: https://doi.org/10.3390/fluids3030059.

[7] – T.-T. Nguyen and D. Byun, “Two-Dimensional Aerodynamic Models of Insect Flight for Robotic Flapping Wing Mechanisms of Maximum Efficiency,” *Journal of Bionic Engineering*, vol. 5, no. 1, pp. 1–11, Mar. 2008, doi: https://doi.org/10.1016/s1672-6529(08)60001-3.

[8] – A. Gehrke and K. Mulleners, “Phenomenology and scaling of optimal flapping wing kinematics,” *Bioinspiration & Biomimetics*, vol. 16, no. 2, pp. 026016–026016, Jul. 2020, doi: https://doi.org/10.1088/1748-3190/abd012.

[9] – S. A. Ansari, K. Knowles, and R. Zbikowski, “Insectlike Flapping Wings in the Hover Part II: Effect of Wing Geometry,” *Journal of Aircraft*, vol. 45, no. 6, pp. 1976–1990, Nov. 2008, doi: https://doi.org/10.2514/1.35697.

[10] – A. Chaudhuri, R. T. Haftka, P. Ifju, K. Chang, C. Tyler, and T. Schmitz, “Experimental flapping wing optimization and uncertainty quantification using limited samples,” *Structural and Multidisciplinary Optimization*, vol. 51, no. 4, pp. 957–970, Nov. 2014, doi: https://doi.org/10.1007/s00158-014-1184-x.

[11] – A. R. Shanmugam and Chang Hwan Sohn, “Numerical investigation on thrust production and unsteady mechanisms of three-dimensional oscillating wing,” *Journal of Mechanical Science and Technology*, vol. 33, no. 12, pp. 5889–5900, Dec. 2019, doi: https://doi.org/10.1007/s12206-019-1134-z.

[12] – D. Diaz-Arriba, T. Jardin, N. Gourdain, F. Pons, and L. David, “Experiments and numerical simulations on hovering three-dimensional flexible flapping wings,” *Bioinspiration & Biomimetics*, vol. 17, no. 6, p. 065006, Oct. 2022, doi: https://doi.org/10.1088/1748-3190/ac8f06.

[13] – D. Diaz-Arriba, T. Jardin, N. Gourdain, F. Pons, and L. David, “Experiments and numerical simulations on hovering three-dimensional flexible flapping wings,” *Bioinspiration & Biomimetics*, vol. 17, no. 6, p. 065006, Oct. 2022, doi: https://doi.org/10.1088/1748-3190/ac8f06.

[14] – W. R. Roderick, M. R. Cutkosky, and D. Lentink, “Touchdown to take-off: at the interface of flight and surface locomotion,” *Interface Focus*, vol. 7, no. 1, pp. 20160094–20160094, Feb. 2017, doi: https://doi.org/10.1098/rsfs.2016.0094.

[15] – S. K. CHATURVEDI, N. C. A. VISHWATH, H. VERMA, and T. MANCHANDA, “Unmanned aero-amphibious vehicle: preliminary study on conceptual design,” *INCAS BULLETIN*, vol. 11, no. 3, pp. 41–53, Sep. 2019, doi: https://doi.org/10.13111/2066-8201.2019.11.3.4.

[16] – J. Izraelevitz and M. S. Triantafyllou, “A novel degree of freedom in flapping wings shows promise for a dual aerial/aquatic vehicle propulsor,” *arXiv (Cornell University)*, May 2015, doi: https://doi.org/10.1109/icra.2015.7140015.

[17] – O. Ozcan, H. Wang, J. D. Taylor, and M. Sitti, “STRIDE II: A Water Strider-inspired Miniature Robot with Circular Footpads,” *International Journal of Advanced Robotic Systems*, vol. 11, no. 6, p. 85, Jan. 2014, doi: https://doi.org/10.5772/58701.

[18] – J. Moore, A. Fein, and W. Setzler, “Design and Analysis of a Fixed-Wing Unmanned Aerial-Aquatic Vehicle,” *2018 IEEE International Conference on Robotics and Automation (ICRA)*, May 2018, doi: https://doi.org/10.1109/icra.2018.8461240.

[19] – W. Weisler, W. Stewart, M. B. Anderson, K. J. Peters, A. Gopalarathnam, and M. Bryant, “Testing and Characterization of a Fixed Wing Cross-Domain Unmanned Vehicle Operating in Aerial and Underwater Environments,” *IEEE Journal of Oceanic Engineering*, vol. 43, no. 4, pp. 969–982, Oct. 2018, doi: https://doi.org/10.1109/joe.2017.2742798.

[20] – W. Stewart *et al.*, “Design and demonstration of a seabird-inspired fixed-wing hybrid UAV-UUV system,” *Bioinspiration & Biomimetics*, vol. 13, no. 5, p. 056013, Aug. 2018, doi: https://doi.org/10.1088/1748-3190/aad48b.

[21] – A. Villegas, V. Mishkevich, Y. Gulak, and F. J. Diez, “Analysis of key elements to evaluate the performance of a multirotor unmanned aerial–aquatic vehicle,” *Aerospace Science and Technology*, vol. 70, pp. 412–418, Nov. 2017, doi: https://doi.org/10.1016/j.ast.2017.07.046.

[22] – D. Lu *et al.*, “Design, fabrication, and characterization of a multimodal hybrid aerial underwater vehicle,” *Ocean Engineering*, vol. 219, p. 108324, Jan. 2021, doi: https://doi.org/10.1016/j.oceaneng.2020.108324.

[23] – A. Farinha, Julien di Tria, R. Zufferey, S. F. Armanini, and M. Kovac, “Challenges in Control and Autonomy of Unmanned Aerial-Aquatic Vehicles,” *Mediterranean Conference on Control and Automation*, Jun. 2021, doi: https://doi.org/10.1109/med51440.2021.9480342.

[24] – Xinyan Deng, L. Schenato, Wei Chung Wu, and S. S. Sastry, “Flapping flight for biomimetic robotic insects: part I-system modeling,” *IEEE Transactions on Robotics*, vol. 22, no. 4, pp. 776–788, Aug. 2006, doi: https://doi.org/10.1109/tro.2006.875480.

[25] – Y. M. Chukewad, J. James, A. Singh, and S. Fuller, “RoboFly: An Insect-Sized Robot With Simplified Fabrication That Is Capable of Flight, Ground, and Water Surface Locomotion,” *IEEE Transactions on Robotics*, vol. 37, no. 6, pp. 2025–2040, Dec. 2021, doi: https://doi.org/10.1109/tro.2021.3075374.

[26] – P. Gopalakrishnan and D. K. Tafti, “Effect of Wing Flexibility on Lift and Thrust Production in Flapping Flight,” *AIAA Journal*, vol. 48, no. 5, pp. 865–877, May 2010, doi: https://doi.org/10.2514/1.39957.

[27] – T. Hesselberg, “Sensors and control systems for micro-air vehicles: lessons from flies,” *Sensor Review*, vol. 29, no. 2, pp. 120–126, Mar. 2009, doi: https://doi.org/10.1108/02602280910936228.

[28] – “STM23S-3RE | Applied Motion,” *www.applied-motion.com*. https://www.applied-motion.com/products/integrated-steppers/stm23s-3re (accessed May 03, 2023).

[29] – “M201624 2 MOD - 1.5 Ratio - 16/24 Teeth Metric Precision Bevel Gears - Steel EN8,” *Bolton Engineering Products Ltd - Bearing, Power Transmission & Workwear Supplier*. https://bepltd.com/products/2-mod-1-5-ratio-16-24-teeth-precision-bevel-gears-steel-en8 (accessed May 03, 2023).

[30] – “ATI Industrial Automation: F/T Sensor Nano17,” *www.ati-ia.com*. https://www.ati-ia.com/products/ft/ft_models.aspx?id=Nano17

[31] – “RE PLANETARY GEARBOX RE34 PLANETARY GEARBOX.” Accessed: May 04, 2023. [Online]. Available: https://motioncontrolproducts.com/media/productattach/r/e/re-planetary-gearbox.pdf

[32] – “Jaw Couplings: Curved for Zero-Backlash | Ruland,” *Ruland.com*, 2015. https://www.ruland.com/servo-couplings/jaw-couplings.html (accessed Nov. 10, 2019).

[33] – Properties: Stainless Steel - Grade 316 (UNS S31600, “Properties: Stainless Steel - Grade 316 (UNS S31600),” *AZoM.com*, 2019. https://www.azom.com/properties.aspx?ArticleID=863

[34] – “Aluminum,” *www.mit.edu*. https://www.mit.edu/~6.777/matprops/aluminum.htm

[35] – Wake structure and aerodynamic performance of low aspect-ratio revolving plates at low reynolds number - Scientific Figure on ResearchGate. Available from: https://www.researchgate.net/figure/a-Lift-and-drag-coefficient-of-rotational-cases-for-a-rectangular-plate-of-AR2-at_fig4_286411007 (accessed 3 May, 2023)

[36] – “Torsion of a Shaft under the Action of Two Torques,” *autofem.com*. https://autofem.com/examples/torsion_of_shaft_with_circular_cross_section_under_2_torques.html

[37] – Mouser, “Connective Peripherals ES-U-3001-M,” *Mouser Electronics*, 2023. https://www.mouser.co.uk/ProductDetail/Connective-Peripherals/ES-U-3001-M?qs=jotIDw4kbYV9GiEaKLbLDA%3D%3D (accessed May 18, 2023).

[38] – ATI, “F/T Sensor Data Acquisition (DAQ) Systems.” https://www.ati-ia.com/app_content/documents/9620-05-DAQ.pdf (accessed May 18, 2023).

[39] – “Simply Bearings Ltd,” *simplybearings.co.uk*. https://simplybearings.co.uk/shop/p20194084/P12-5M-15F-5mm-Pitch-12-Tooth-Flanged-HTD-Type-Steel-Timing-Pulley-for-15mm-Wide-Belts/product_info.html (accessed May 03, 2023).

[40] – “4 Hole Flange Bearing Unit 30mm ID | RS,” *uk.rs-online.com*. https://uk.rs-online.com/web/p/bearing-units/7508784 (accessed May 04, 2023).

8. Appendices:

Appendix A:

Table 1 Effect of types of rotation in hovering flight with rotation axis at quarter-chord position

α_{s0}	$J=0$	C_v	C_h	C_p
	Symmetrical rotation		$\beta=0^\circ$	
21°28	Translation down	1.22	−0.49	0.56
	Supination	0.55	−1.44	1.06
21°28	Translation up	1.22	0.49	0.56
	Pronation	0.55	1.44	1.06
	Full-cycle average	1.00	0.00	0.72
	Advanced rotation		$\beta=0^\circ$	
24°30	Translation down	1.50	−0.68	0.77
	Supination	0.01	−3.81	6.80
24°30	Translation up	1.50	0.68	0.77
	Pronation	0.01	3.81	6.80
	Full-cycle average	1.00	0.00	2.78
	Delayed rotation		$\beta=0^\circ$	
25°78	Translation down	1.62	−0.78	0.88
	Supination	−0.24	−0.35	0.08
25°78	Translation up	1.62	0.78	0.88
	Pronation	−0.24	0.35	0.08
	Full-cycle average	1.00	0.00	0.62

Table 2 Effect of types of rotation in hovering flight with rotation axis at mid-chord position

α_{s0}	$J=0$	C_v	C_h	C_p
	Symmetrical rotation		$\beta=0^\circ$	
22°04	Translation down	1.30	−0.53	0.61
	Supination	0.41	0.00	0.28
22°04	Translation up	1.30	0.53	0.61
	Pronation	0.41	0.00	0.28
	Full-cycle average	1.00	0.00	0.50
	Advanced rotation		$\beta=0^\circ$	
24°55	Translation down	1.52	−0.69	0.79
	Supination	−0.04	0.79	0.62
24°55	Translation up	1.52	0.69	0.79
	Pronation	−0.04	−0.79	0.62
	Full-cycle average	1.00	0.00	0.73
	Delayed rotation		$\beta=0^\circ$	
24°55	Translation down	1.52	−0.69	0.79
	Supination	−0.04	0.79	0.62
24°55	Translation up	1.52	0.69	0.79
	Pronation	−0.04	−0.79	0.62
	Full-cycle average	1.00	0.00	0.73

Tables showing the effect of changing the pitch axis from mid-chord to quarter-chord position [6]

Appendix B:

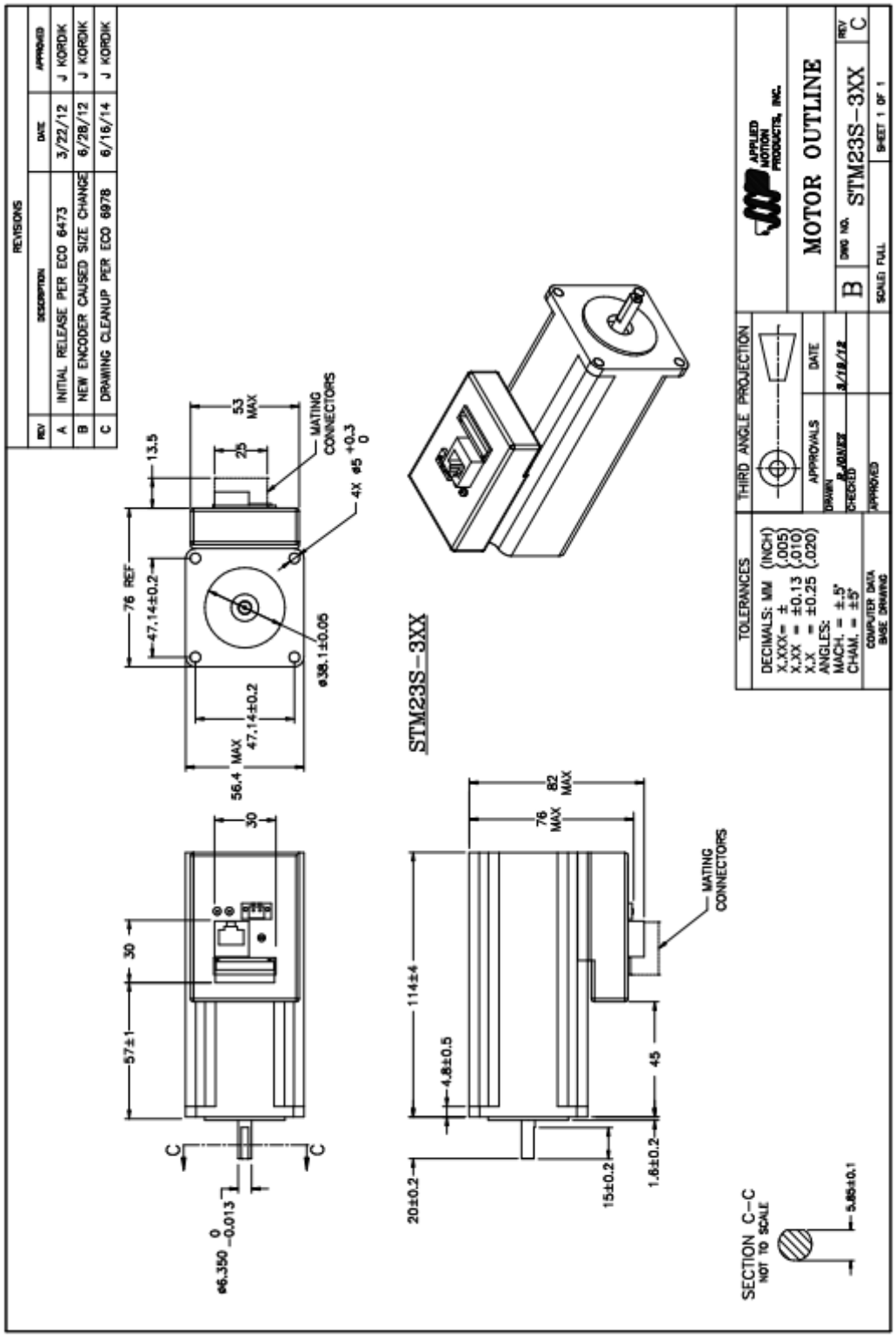
REVISIONS
REV
DESCRIPTION
DATE
APPROVED
A
INITIAL RELEASE PER ECO 6473
3/22/12
J KORDIK
B
NEW ENCODER CAUSED SIZE CHANGE
6/28/12
J KORDIK
C
DRAWING CLEANUP PER ECO 6978
6/16/14
J KORDIK
MOTOR OUTLINE
STM23S-3XX
MATING CONNECTORS
SECTION C-C
NOT TO SCALE
THIRD ANGLE PROJECTION
TOLERANCES
APPLIED MOTION PRODUCTS, INC.

Appendix C:

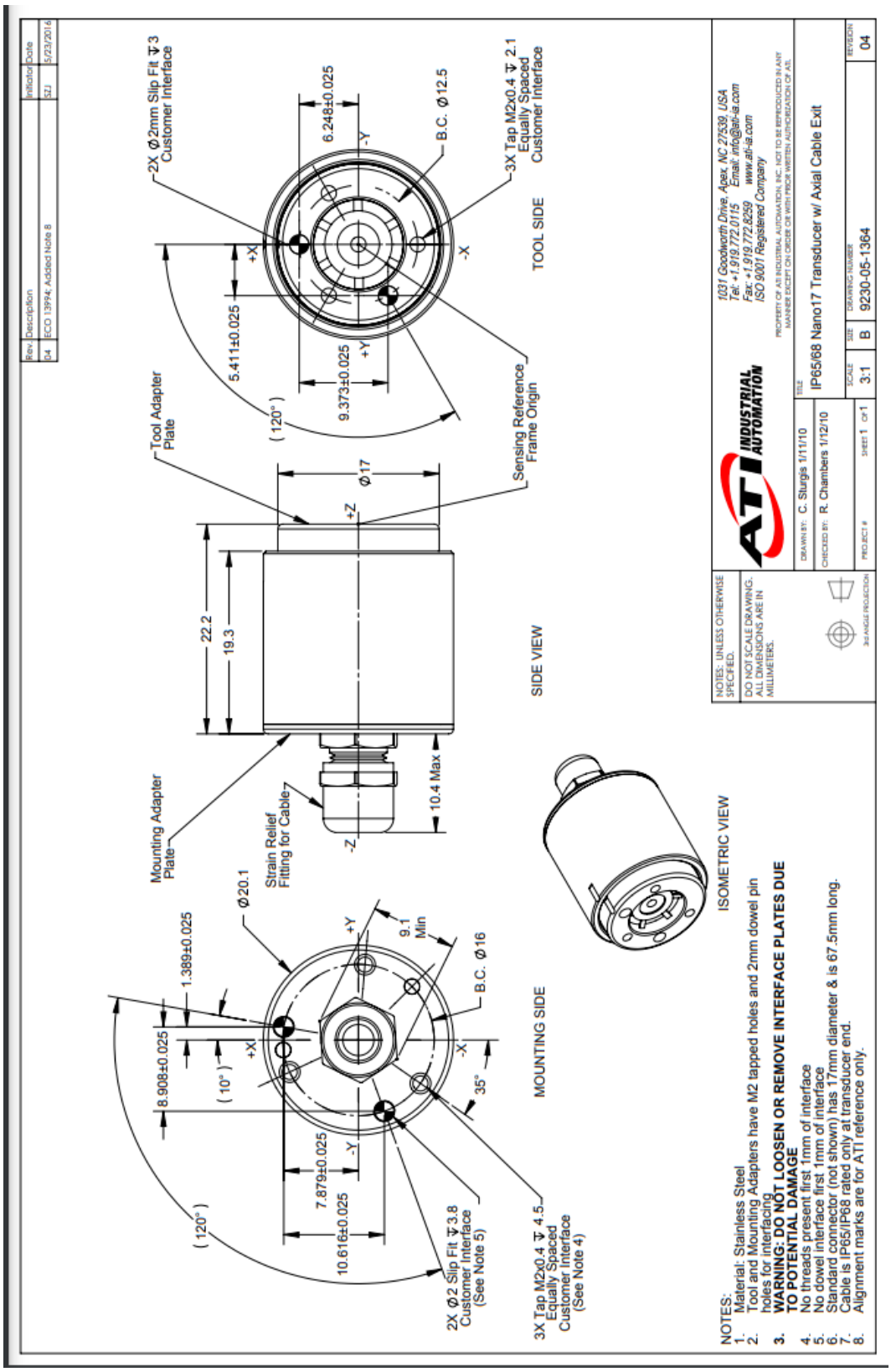
Rev Description Initials Date
04 ECO 13994; Added Note 8 SZJ 5/23/2016
2X Ø2mm Slip Fit ∓3
Customer Interface
6.248±0.025
B.C. Ø12.5
3X Tap M2x0.4 ∓ 2.1
Equally Spaced
Customer Interface
TOOL SIDE
Tool Adapter
Plate
5.411±0.025
(120°)
9.373±0.025
Sensing Reference
Frame Origin
Ø17
+Z
22.2
19.3
Mounting Adapter
Plate
Strain Relief
Fitting for Cable
10.4 Max
-Z
SIDE VIEW
Ø20.1
1.389±0.025
9.1
Min
B.C. Ø16
8.908±0.025
(10°)
35°
7.879±0.025
10.616±0.025
(120°)
2X Ø2 Slip Fit ∓3.8
Customer Interface
(See Note 5)
3X Tap M2x0.4 ∓ 4.5
Equally Spaced
Customer Interface
(See Note 4)
MOUNTING SIDE
ISOMETRIC VIEW
NOTES:
1. Material: Stainless Steel
2. Tool and Mounting Adapters have M2 tapped holes and 2mm dowel pin holes for interfacing
3. WARNING: DO NOT LOOSEN OR REMOVE INTERFACE PLATES DUE TO POTENTIAL DAMAGE
4. No threads present first 1mm of interface
5. No dowel interface first 1mm of interface
6. Standard connector (not shown) has 17mm diameter & is 67.5mm long.
7. Cable is IP65/IP68 rated only at transducer end.
8. Alignment marks are for ATI reference only.
NOTES: UNLESS OTHERWISE SPECIFIED.
DO NOT SCALE DRAWING. ALL DIMENSIONS ARE IN MILLIMETERS.
INDUSTRIAL AUTOMATION
1031 Goodworth Drive, Apex, NC 27539, USA
Tel: +1.919.772.0115 Email: info@ati-ia.com
Fax: +1.919.772.8259 www.ati-ia.com
ISO 9001 Registered Company
PROPERTY OF ATI INDUSTRIAL AUTOMATION, INC. NOT TO BE REPRODUCED IN ANY MANNER EXCEPT ON ORDER OR WITH PRIOR WRITTEN AUTHORIZATION OF ATI.
DRAWN BY: C. Sturgis 1/11/10
CHECKED BY: R. Chambers 1/12/10
PROJECT #
SHEET 1 OF 1
3rd ANGLE PROJECTION
TITLE
IP65/68 Nano17 Transducer w/ Axial Cable Exit
SCALE 3:1
SIZE B
DRAWING NUMBER 9230-05-1364
REVISION 04

Appendix D:

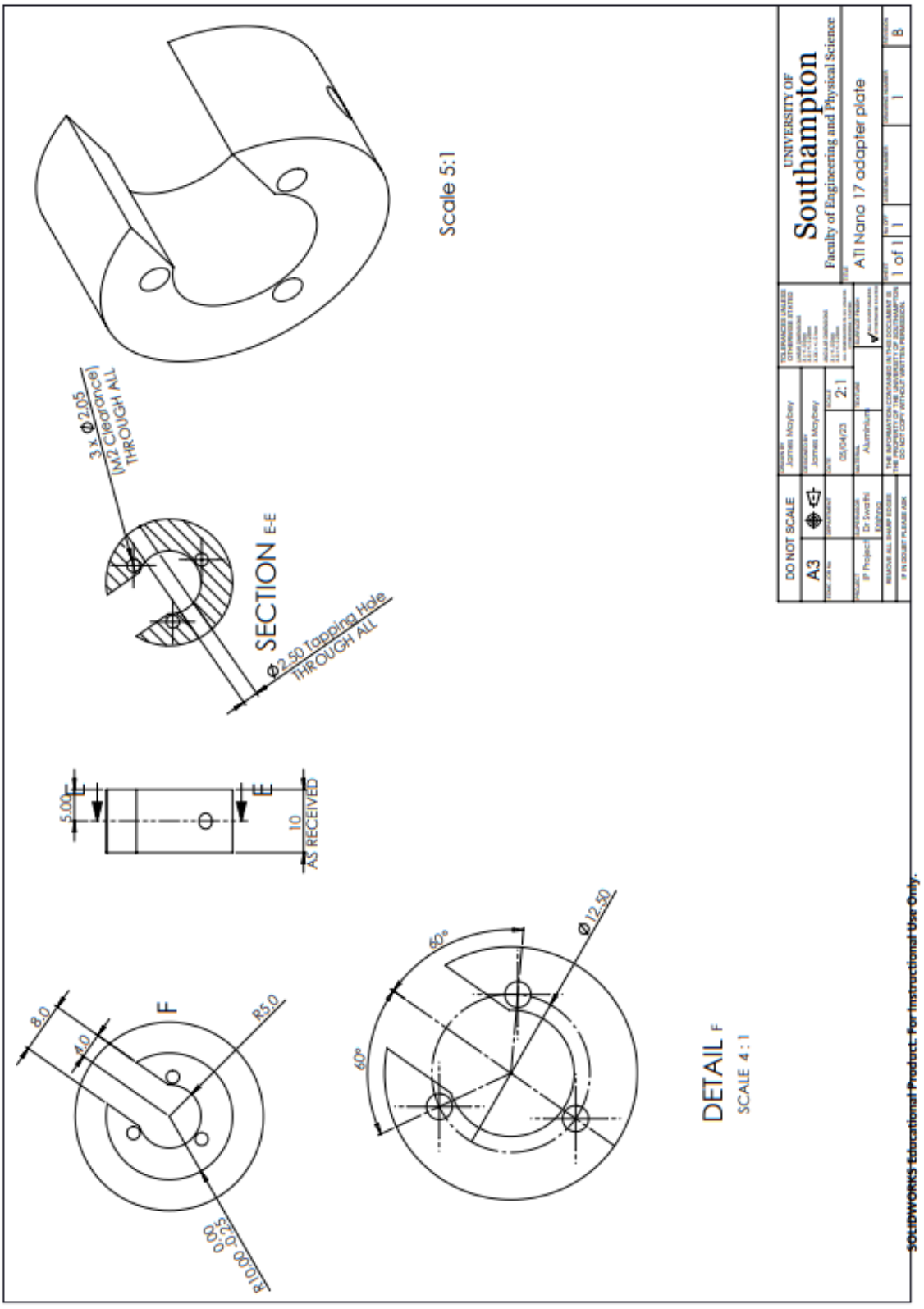
Scale 5:1
3 x Φ2.05 (M2 Clearance) THROUGH ALL
SECTION E-E
Φ2.50 Tapping Hole THROUGH ALL
5.00
10
AS RECEIVED
DETAIL F
SCALE 4 : 1
8.0
4.0
R5.0
R10.00
0.00
-0.25
60°
60°
Ø12.50
DO NOT SCALE
A3
UNIVERSITY OF Southampton
Faculty of Engineering and Physical Science
Alt Nano 17 adapter plate
1 of 1
B
SOLIDWORKS Educational Product. For Instructional Use Only.

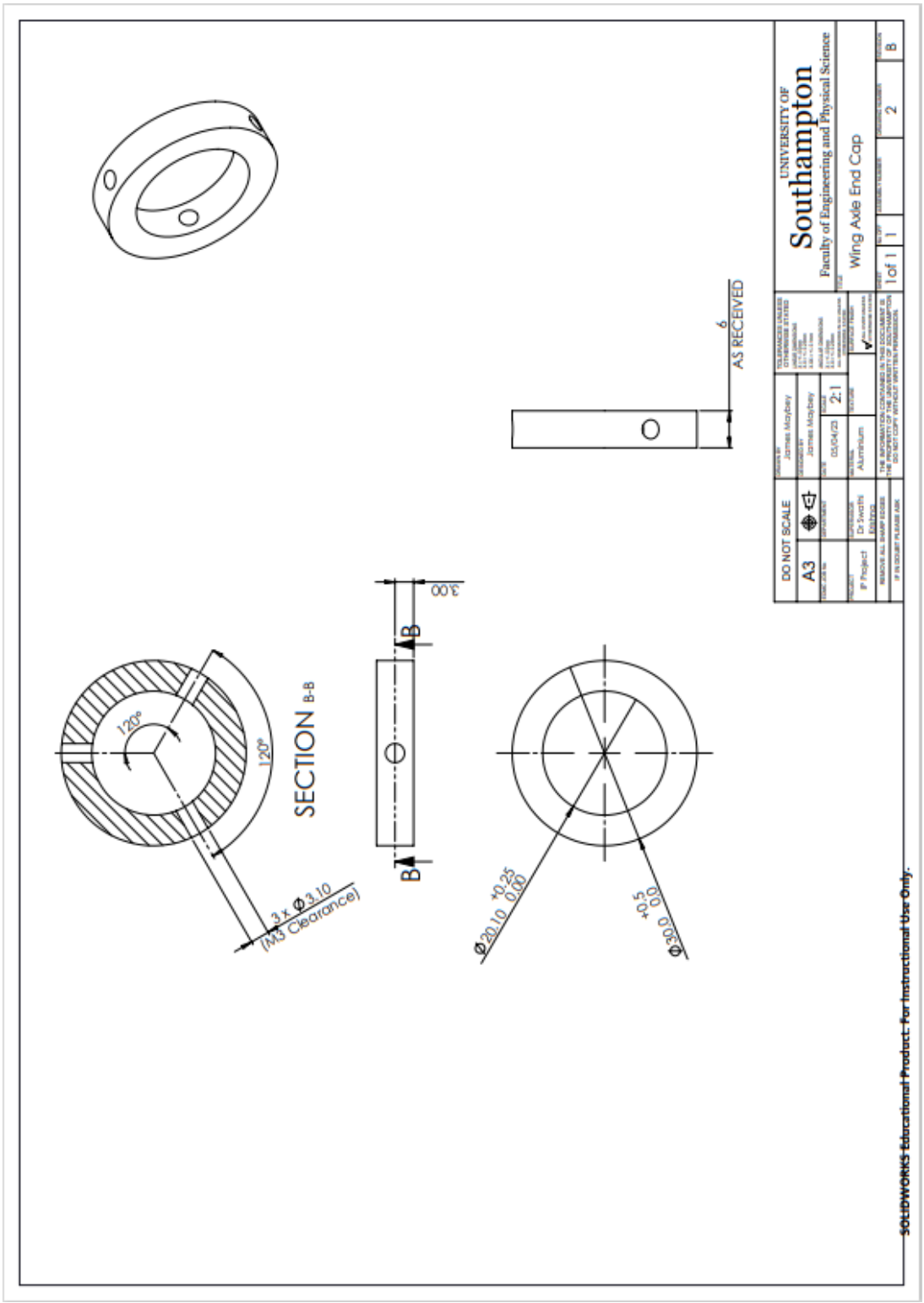
AS RECEIVED
SECTION B-B
120°
120°
3 x Φ3.10
(M3 Clearance)
3.00
B
B
Φ20.10 +0.25 0.00
Φ30.0 +0.5 0.0
DO NOT SCALE
A3
Southampton
Faculty of Engineering and Physical Science
Wing Axle End Cap
James Maybey
05/04/23
2:1
Aluminium
1 of 1
2
B
SOLIDWORKS Educational Product. For Instructional Use Only.

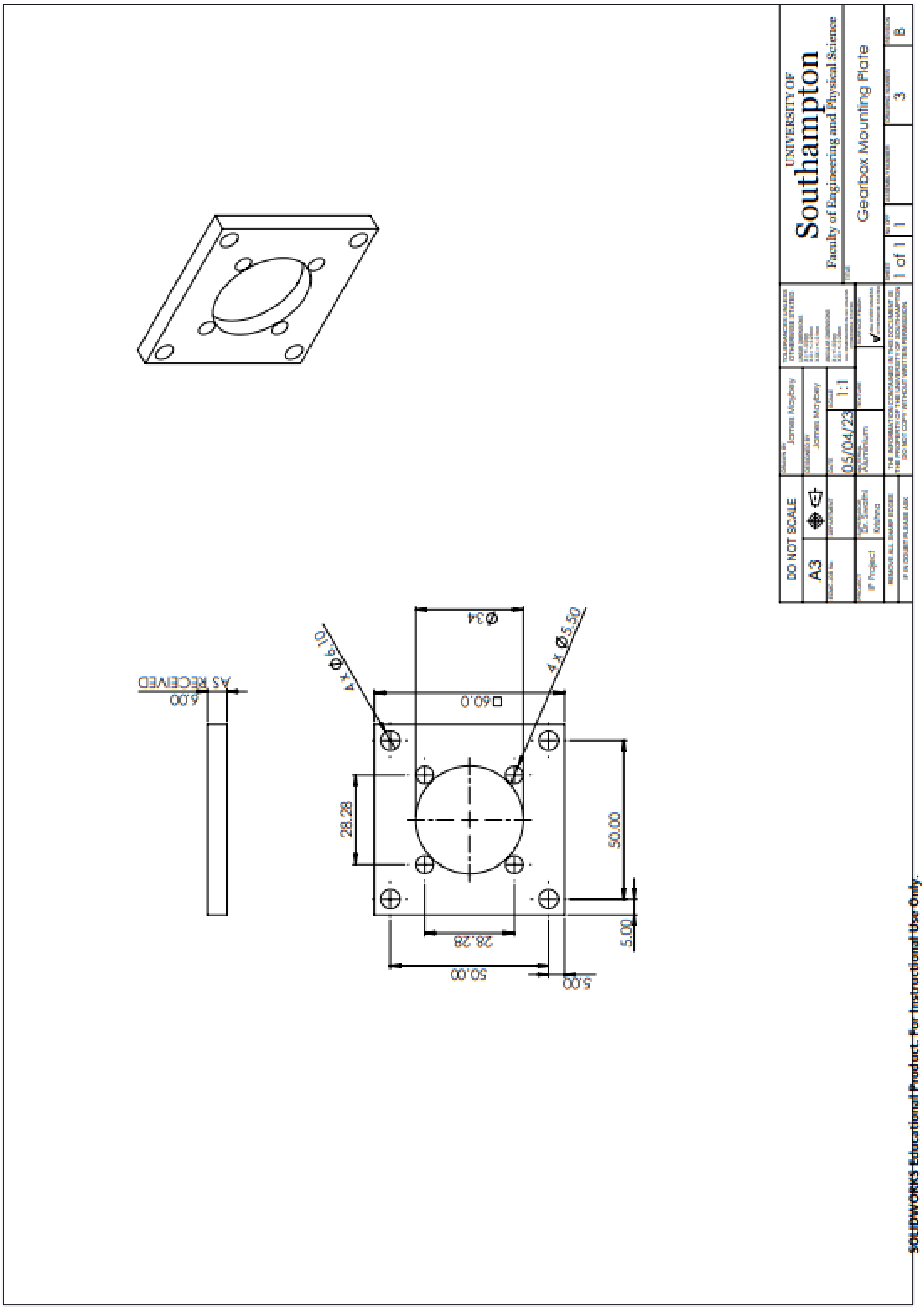
UNIVERSITY OF
Southampton
Faculty of Engineering and Physical Science
Gearbox Mounting Plate
DO NOT SCALE
A3
James Maybey
05/04/23
1:1
Aluminium
IP Project
1 of 1
3
B
□60.0
Ø34
4 X Ø5.50
4 X Ø6.10
28.28
50.00
5.00
6.00
AS RECEIVED
SOLIDWORKS Educational Product. For Instructional Use Only.

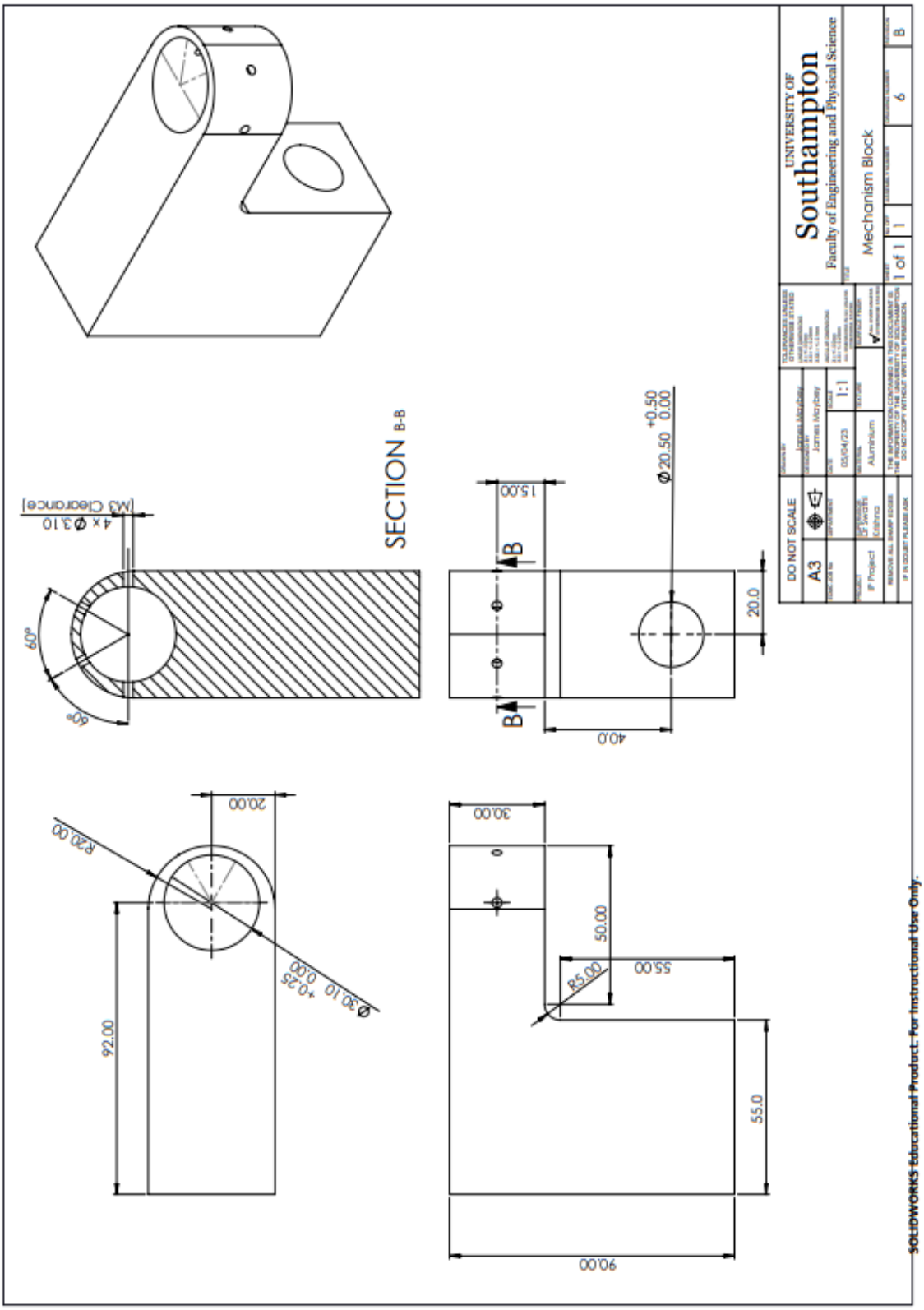
UNIVERSITY OF
Southampton
Faculty of Engineering and Physical Science
Mechanism Block
DO NOT SCALE
A3
SECTION B-B
4 x Ø 3.10
M3 Clearance
60°
60°
15.00
B
B
Ø 20.50 +0.50 0.00
20.0
40.0
20.00
R20.00
Ø 30.10 +0.25 0.00
92.00
30.00
50.00
R5.00
55.00
55.0
90.00
SOLIDWORKS Educational Product. For Instructional Use Only.

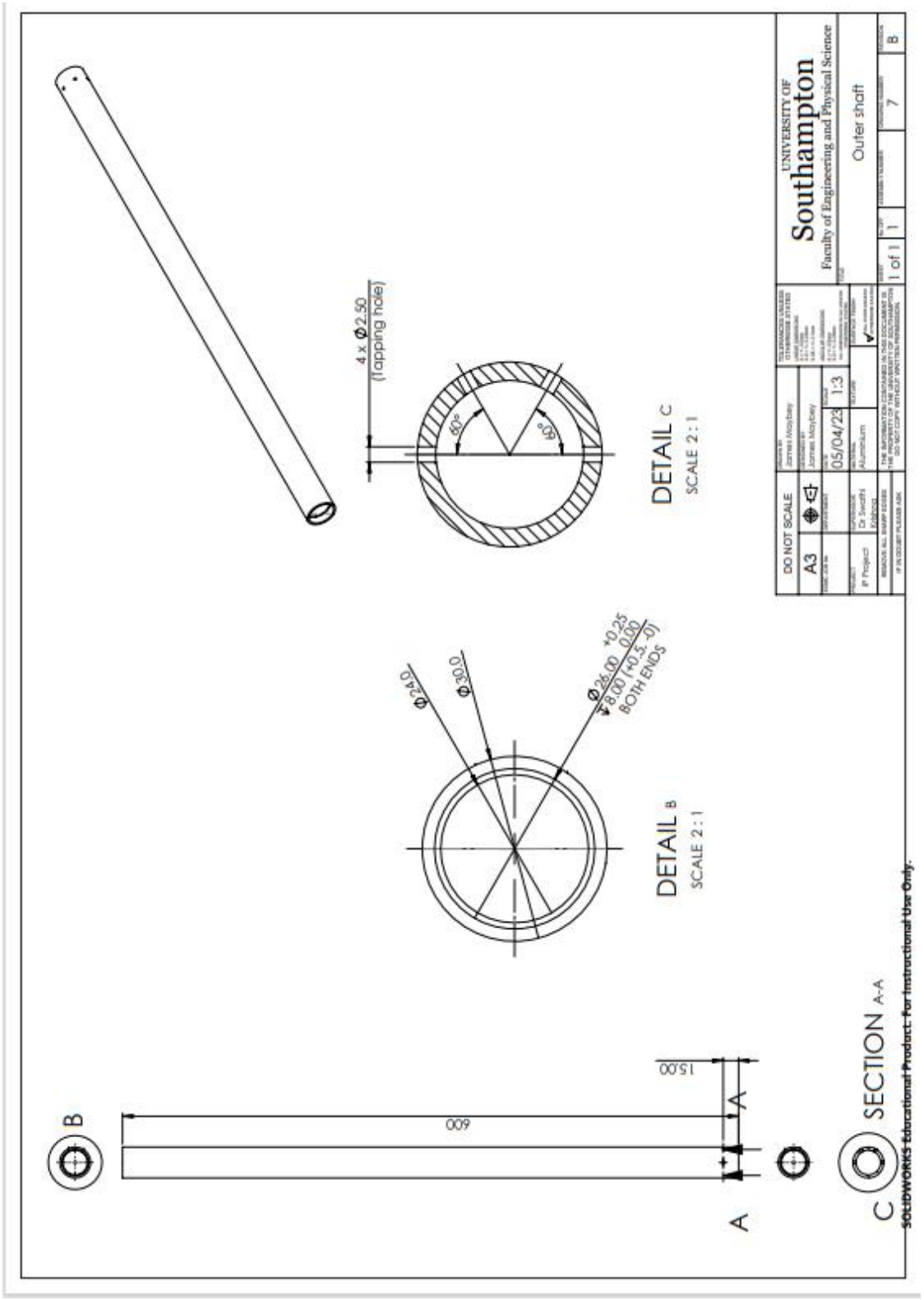
4 x Ø2.50
(tapping hole)
60°
60°
DETAIL C
SCALE 2 : 1
Ø24.0
Ø30.0
Ø26.00 +0.25 -0.00
8.00 (+0.5, -0)
BOTH ENDS
DETAIL B
SCALE 2 : 1
600
15.00
A
A
B
C
SECTION A-A
DO NOT SCALE
A3
Southampton
Faculty of Engineering and Physical Science
Outer shaft
05/04/23
1:3
Aluminium
1 of 1
7
B
SOLIDWORKS Educational Product. For Instructional Use Only.

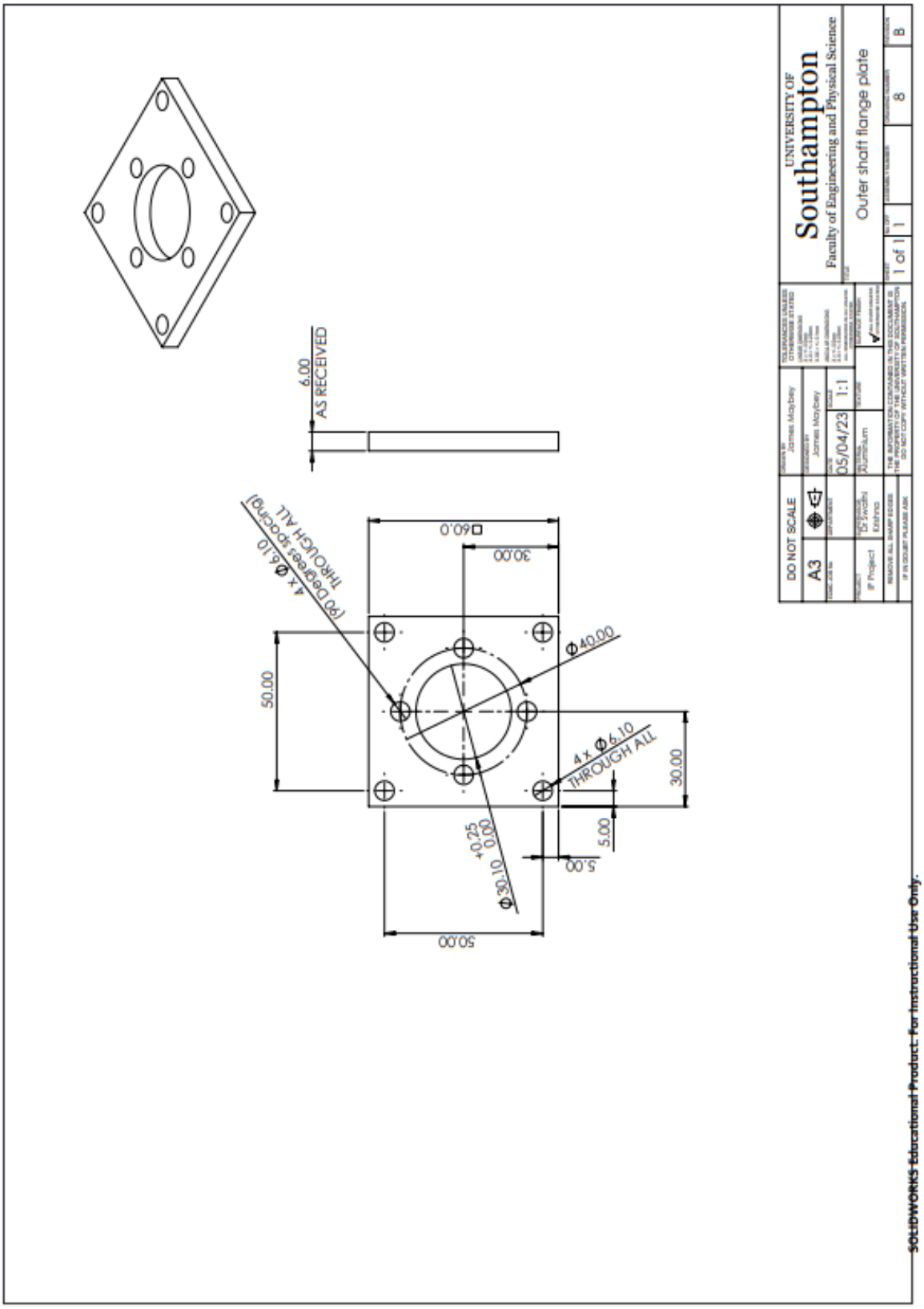
6.00
AS RECEIVED
□60.0
30.00
4 x Ø6.10
(90 Deg Countersunk)
THROUGH ALL
Ø40.00
50.00
4 x Ø6.10
THROUGH ALL
30.00
5.00
5.00
Ø30.10 +0.25 0.00
50.00
DO NOT SCALE
A3
UNIVERSITY OF
Southampton
Faculty of Engineering and Physical Science
Outer shaft flange plate
1 of 1
8
B
SOLIDWORKS Educational Product. For Instructional Use Only.

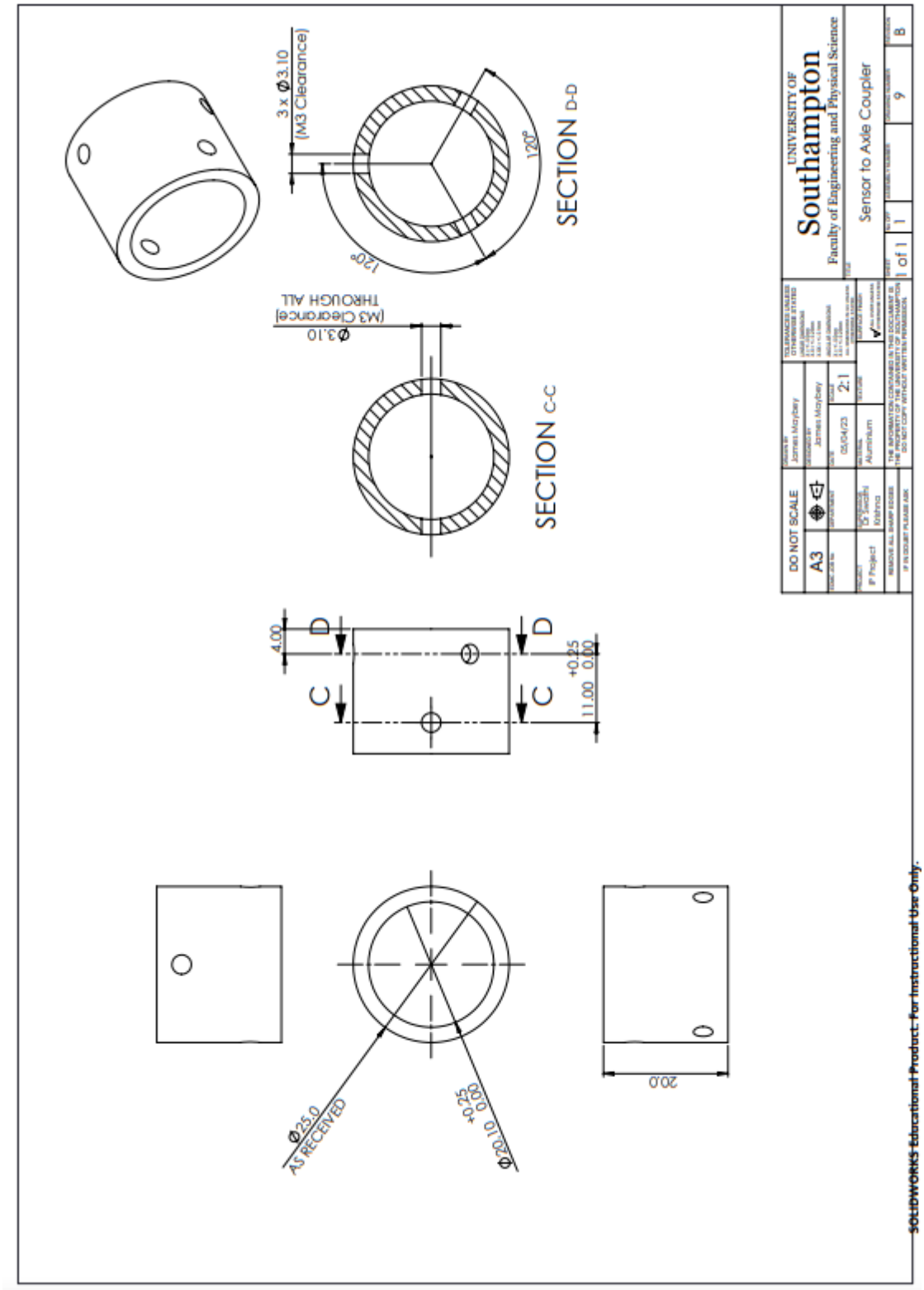
3 x Ø3.10
(M3 Clearance)
120°
120°
SECTION D-D
Ø3.10
(M3 Clearance)
THROUGH ALL
SECTION C-C
4.00
D
D
C
C
+0.25
11.00 0.00
Ø25.0
AS RECEIVED
+0.25
Ø20.10 0.00
20.0
DO NOT SCALE
A3
IF Project
Aluminium
2:1
02/04/23
James Maybey
Sensor to Axle Coupler
1 of 1
B
SOLIDWORKS Educational Product. For Instructional Use Only.

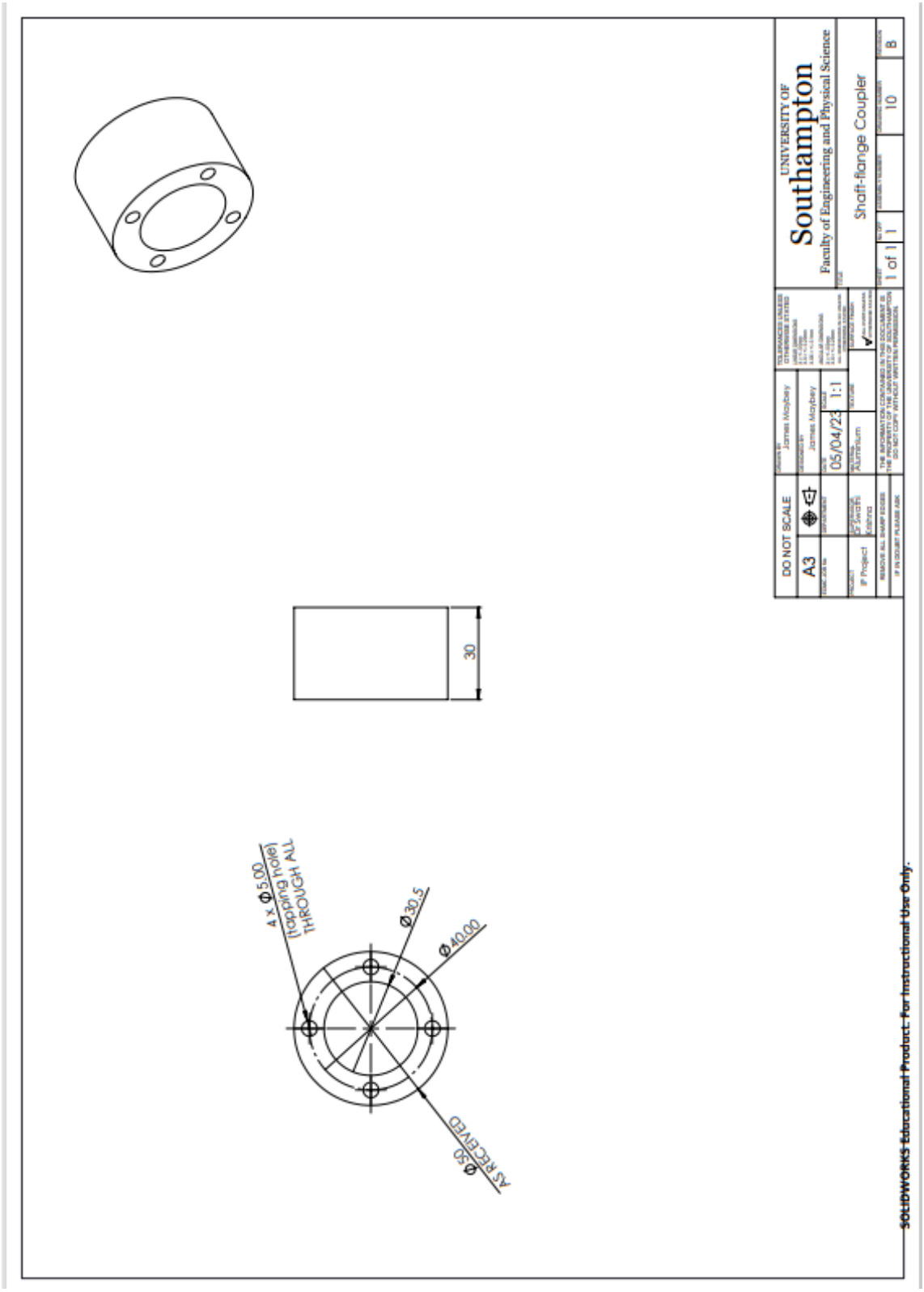
UNIVERSITY OF
Southampton
Faculty of Engineering and Physical Science
Shaft-flange Coupler
DO NOT SCALE
A3
James Maybey
05/04/23
1:1
Aluminium
1 of 1
10
B
30
4 x Ø5.00
(tapping hole)
THROUGH ALL
Ø30.5
Ø40.00
Ø50
AS RECEIVED
SOLIDWORKS Educational Product. For Instructional Use Only.

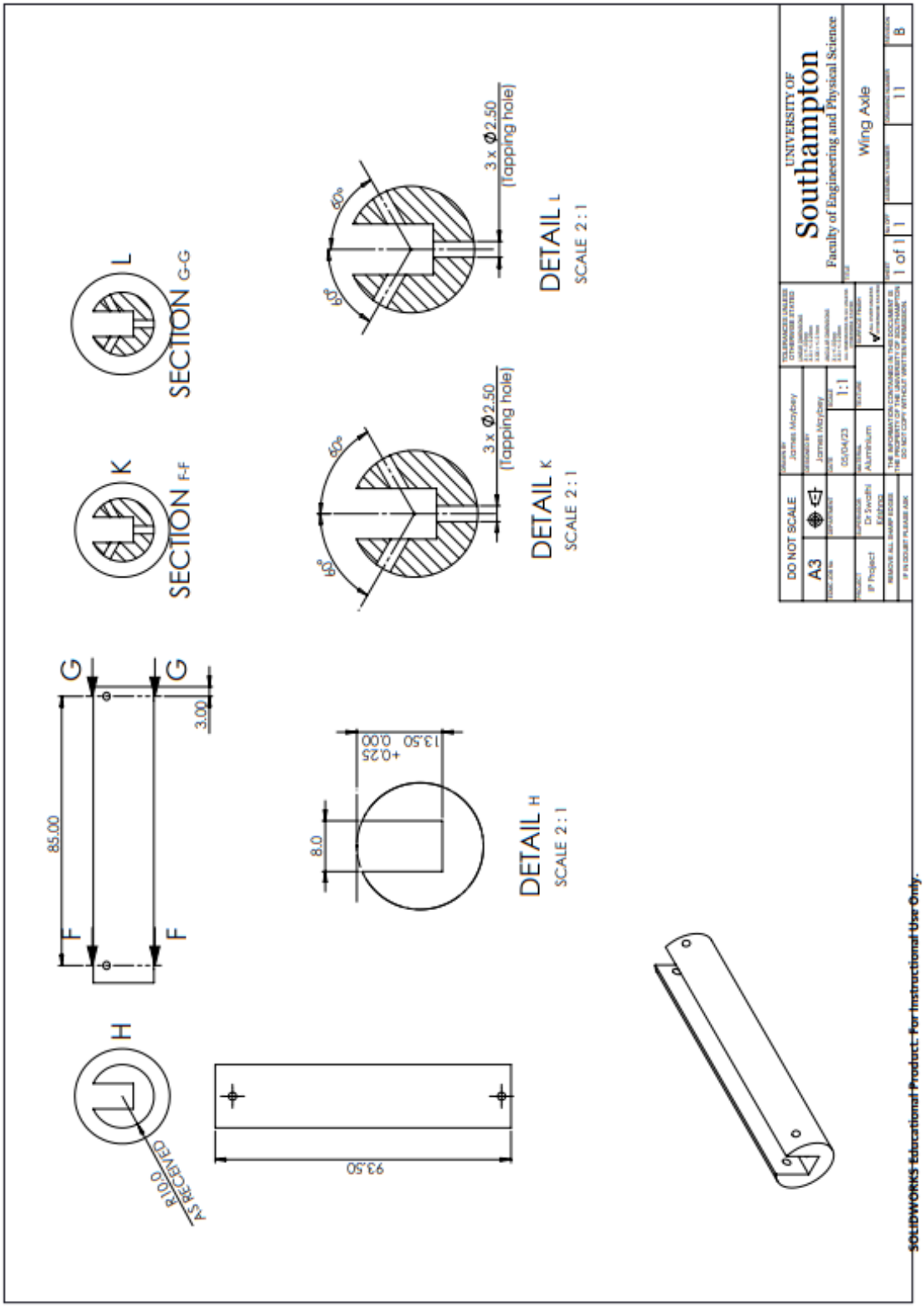
SECTION F-F
SECTION G-G
DETAIL K
SCALE 2 : 1
DETAIL L
SCALE 2 : 1
DETAIL H
SCALE 2 : 1
3 x Ø2.50
(Tapping hole)
85.00
3.00
8.0
93.50
R10.00
AS REQUIRED
DO NOT SCALE
A3
Aluminium
1:1
Wing Axle
Faculty of Engineering and Physical Science
UNIVERSITY OF
Southampton
SOLIDWORKS Educational Product. For Instructional Use Only.

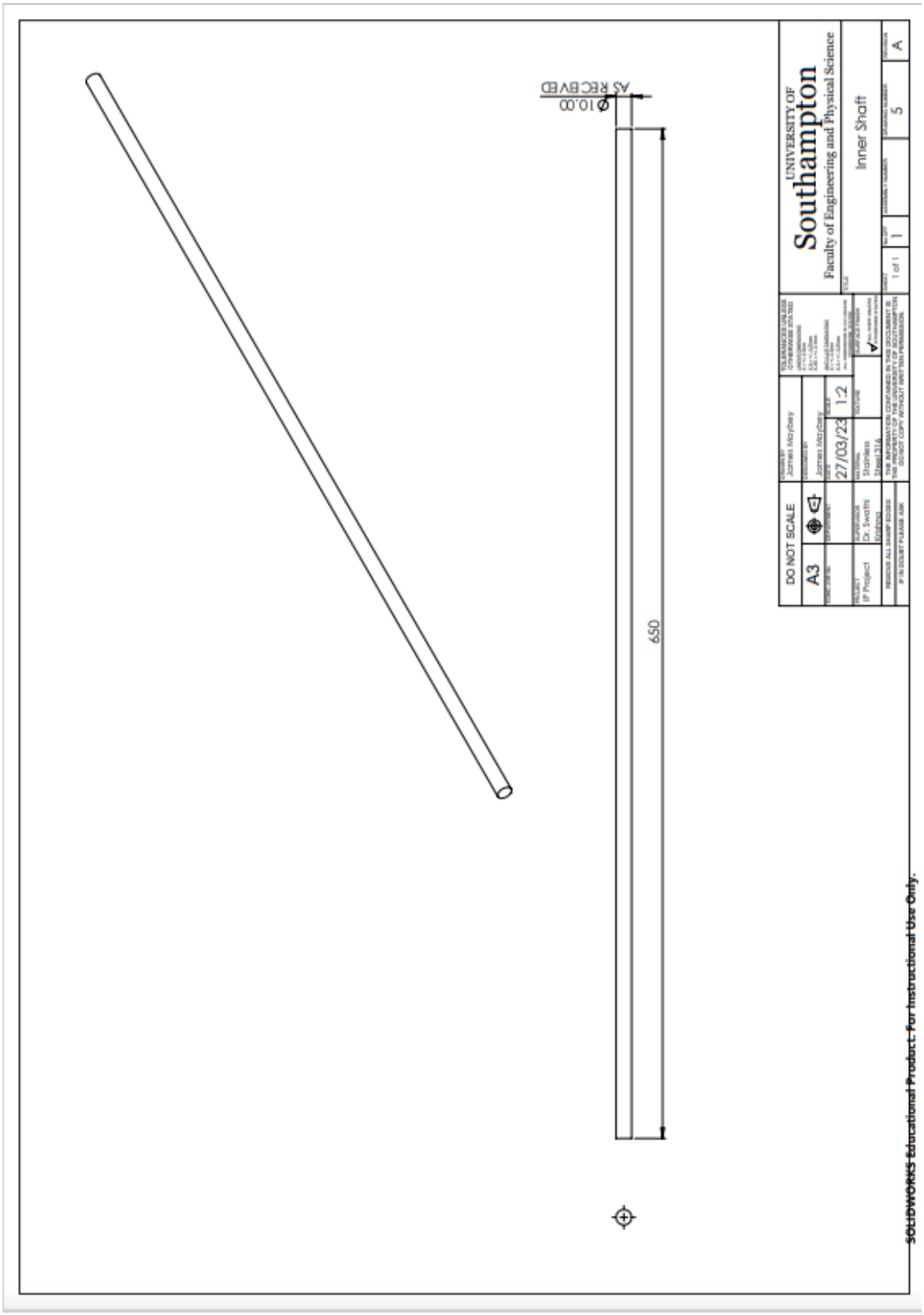
Ø10.00
AS REC BY ED
650
DO NOT SCALE
A3
27/03/23
1:2
Stainless Steel 316
Dr. Sverthi Krishna
IF Project
James Maybey
UNIVERSITY OF Southampton
Faculty of Engineering and Physical Science
Inner Shaft
5
A
1 of 1
SOLIDWORKS Educational Product. For Instructional Use Only.

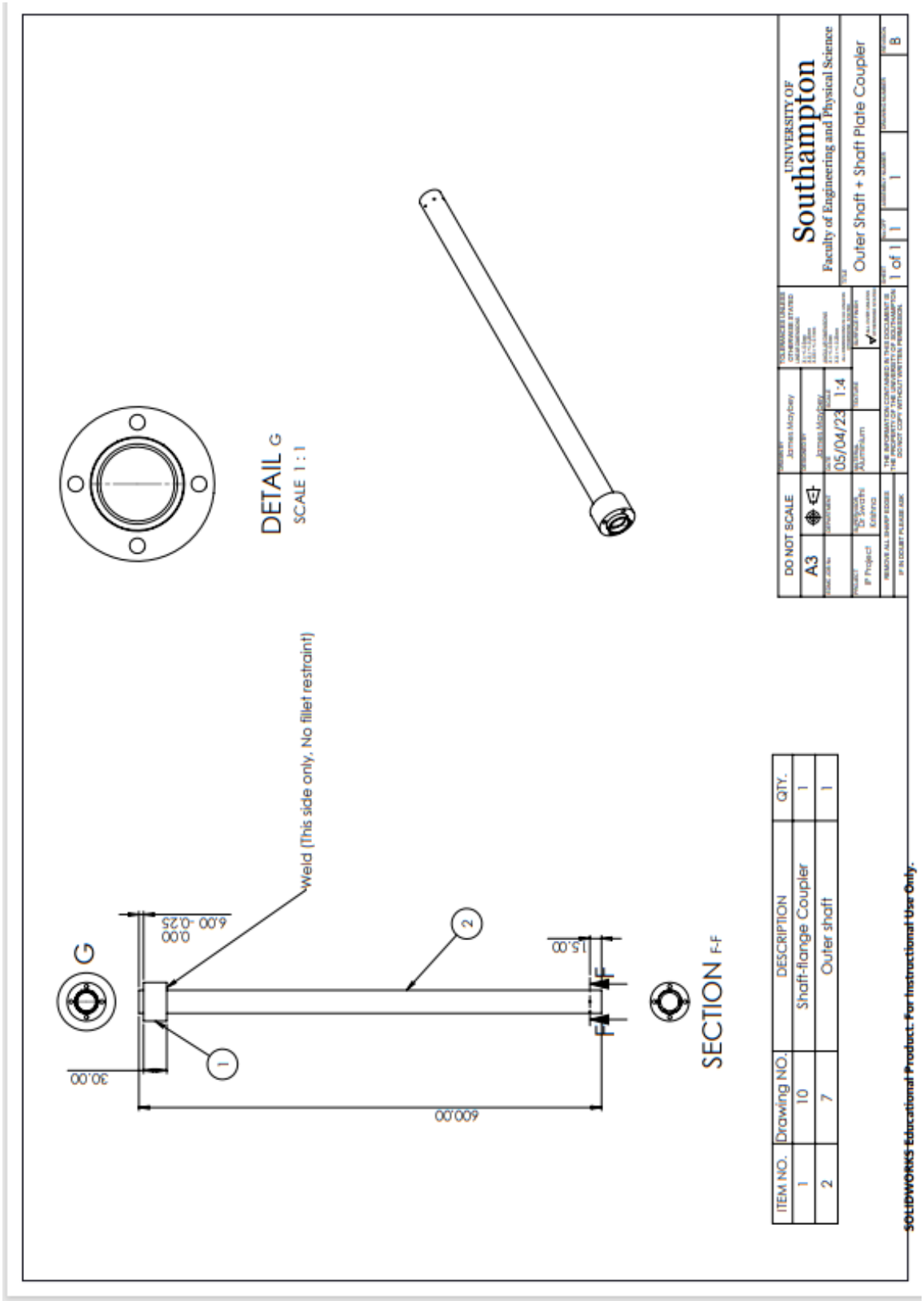
DETAIL G
SCALE 1 : 1
SECTION F-F
Weld (This side only. No fillet restraint)
600.00
30.00
6.00 -0.25
0.00
15.00
ITEM NO. | Drawing NO. | DESCRIPTION | QTY.
1 | 10 | Shaft-flange Coupler | 1
2 | 7 | Outer shaft | 1
DO NOT SCALE
A3
UNIVERSITY OF Southampton
Faculty of Engineering and Physical Science
Outer Shaft + Shaft Plate Coupler
SOLIDWORKS Educational Product. For Instructional Use Only.

Appendix E:

Step No.	Step	Components involved	Instructions
1	Fix the outer shaft	Welded outer shaft subassembly, Mounting frame, Plywood mounting board, Flange bearing	fix the bearing to the board and the board to the frame with M10 and M8 bolts, then push the outer shaft through the bearing and tighten set screws.
2	insert inner shaft and bearings	inner shaft, alignment bearings x2	push the inner shaft down the outer shaft and place the alignment bearings over the inner shaft and into the ends of the outer shaft
3	Fix the pulley system	Large pulley, small pulley, locking bush, pulley belt, stepper motor	slide the large pulley and bush onto the outer shaft from underneath and tighten the set crews to fix, then place motor onto the board and use set screw to fix the small pulley onto the shaft, then use 4 M4 machine screws to bolt the motor into position whilst tightening the belt in place.
4	Fix the second motor	Gearbox, motor, gearbox plate, outer shaft plate, standoffs x4, Ruland jaw coupler	bolt the shaft plate onto the welded sleeve on the top of the outer shaft using 4 M6 bolts, then secure the 4 standoffs to this plate with 4 more M6 bolts, secure the motor to the gearbox using 4 M5 machine screws and then bolt the gearbox to its plate with 4 M5 bolts, this plate can then lastly be secured to the stands with bolts at the same time the Ruland jaw coupler is aligned and fixed to the inner shaft and gearbox output
5	Create the gear sub assembly	Mechanism block, retention ring, Nano17, sensor back plate, 21mm bore gear, wing axle, coupling sleeve	Firstly, thread the sensor through the retention ring, mechanism block, 21mm bore gear, and coupling sleeve. Then slot the back plate over the sensors wire and fix the plate to the back of the sensor, then slot the wing axle over the wire between the gear and sleeve. Then using M3 screws, fix the sleeve to the back plate and wing axle, then slot the wing axle through the gear and mechanism block and fix to the retention ring, finally tighten the gears set screw to fix into the wing axle
6	Fix the wing to the sensor	wing adapter, wing plate	glue the wing plate into position in the adapter, then screw the adapter onto the sensor using M2 screws
7	fix the gear sub assembly onto the outer shaft	driving gear	putting the driving gear into its final position next to the driven gear allows for the assembly to be slid onto the bottom of the outer shaft and the inner shaft can pass into the driving gear whilst the outer shaft stays in the mechanism block, the set screw can then be tightened, fixing the gear, and the 4 M3 machine screws can be used to fix the mechanism block onto the outer shaft
8	Mount the apparatus	Testing environment	The mounting frame can then be fixed to the existing frame above the tanks using right-angled brackets
9	Fix the electronics	Wire connections, signal converter	The wiring can then be implemented, from power source to motors and from signal generator to the converters and then also to the motors. The sensor wire can also then be connected into the reading device, signal converters can be screwed onto the wooden board for fixing.